# Cryogenic Treatment Analysis in WEDM of Al2024/Al2O3/W Composite

**Muhammad Huzaifa Raza** ( huzaifa@connect.hku.hk )
University of Hong Kong
**Muhammad Asad Ali**
University of Engineering and Technology
**Waseem Tahir**
University of Engineering and Technology
**Ray Y. Zhong**
The University of Hong Kong
**Nadeem Ahmad Mufti**
University of Engineering and Technology
**Naveed Ahmad**
Al-Yamamah University

**Research Article**

**Keywords:** WEDM, Al2024/Al2O3/W, Squeeze casting, Cryogenic treatment

**Posted Date:** March 17th, 2021

**DOI:** https://doi.org/10.21203/rs.3.rs-292535/v1

# Cryogenic treatment analysis in WEDM of Al2024/$Al_2O_3$/W composite

Muhammad Huzaifa Raza[1]*, Muhammad Asad Ali[2], Waseem Tahir[3], Ray Y. Zhong[1], Nadeem Ahmad Mufti[2]

Naveed Ahmad[4]

[1]Department of Industrial and Manufacturing Systems Engineering, The University of Hong Kong, Pok Fu Lam, Hong Kong

[2]Department of Industrial and Manufacturing Engineering, University of Engineering and Technology, Lahore 54890, Pakistan

[3]Department of Industrial Engineering, University of Engineering and Technology, Taxila 47080, Pakistan

[4]Department of Industrial Engineering, College of Engineering and Architecture, Al-Yamamah University, Riyadh 11512, Saudi Arabia

*Corresponding author

**Muhammad Huzaifa Raza**

*Email:* huzaifa@connect.hku.hk *Contact No.:* +852-41051802

*Address:* 8/F, Haking Wong Building, Department of Industrial and Manufacturing Systems Engineering, The University of Hong Kong, Pok Fu Lam, Hong Kong

## Abstract

Increasing demand for aluminum matrix composites (AMCs) in the manufacturing sector leads to the development of squeeze casted hybrid AMCs bearing superior mechanical attributes. Excessive hardness due to squeeze pressure and the presence of reinforcement particles makes the machining of AMCs challenging and results in excessive tool wear and inadequate surface finish. Wire electric discharge machining (WEDM) process has been preferred over conventional manufacturing processes for the machining of squeeze casted Al2024/$Al_2O_3$/W hybrid composite. This study investigates the selection of the most pertinent wire electrode for the precise machining of Al2024/$Al_2O_3$/W. Simple zinc-coated (NT) and cryogenic treated (CT) brass wire electrodes have been selected for machining. Scanning electron microscope (SEM) analysis of CT wire shows that cryogenic treatment enhances the soundness and stability by reducing microcavities in its microstructure. To analyze the effects of cryogenic treatment, the machining performance of CT wire has been compared with NT wire. Besides wire type, the influence of key input variables has also been analyzed on the imperative response measures including cutting speed (CS), surface roughness (SR) and kerf width (KW) to make the machining process more effective. Microstructural analysis of NT wire depicts a high concentration of micro-voids, micro-cracks, and deep craters, while the surface of CT has been observed relatively fine after the machining.

Comparative analysis of both wire electrodes has declared that CT wire yields 26.96% and 15.10% superior results for CS and SR respectively, and 6.92% deprived results for KW than NT wire.

*Keywords:* WEDM; Al2024/$Al_2O_3$/W; Squeeze casting; Cryogenic treatment

*Nomenclature*

| | |
|---|---|
| WEDM | Wire electric discharge machining |
| AMC | Aluminum matrix composite |
| $T_{ON}$ | Pulse duration |
| $F_R$ | Wire feed rate |
| $S_W$ | Wire runoff speed |
| $T_W$ | Wire tension |
| $T_{OFF}$ | Pulse off time |
| CS | Cutting speed |
| SR | Surface roughness |
| KW | Kerf width |
| I | Discharge current |
| V | Gap voltage |
| SEM | Scanning electron microscope |
| CT wire | Cryogenic treated zinc-coated brass wire |
| NT wire | Non-cryogenic treated zinc-coated brass wire |
| UTS | Ultimate tensile strength |
| RSM | Response surface methodology |
| ANOVA | Analysis of variance |
| GRA | Grey relational analysis |
| GRG | Grey relational grade |

# 1 Introduction

In engineering materials, aluminum is the most alluring material due to its high strength, low weight, formability, recyclability, and corrosion resistance capability. Inadequate wear resistance and deprived performance at elevated temperatures are major concerns of aluminum alloys [1]. These deficiencies are generally overcome by introducing reinforced particles in such alloys to produce aluminum matrix composites (AMCs) [2-5]. Reinforced particles in the metal matrix improve the mechanical characteristics of AMCs by modifying the microstructural attributes. These superior properties of AMCs have enhanced their demand in marine, automotive, defense, and aerospace applications [6]. AMCs are generally fabricated by stir casting process, in which preheated reinforced particles are introduced in the matrix material and mixed uniformly with a mechanical stirrer [7]. Nevertheless, researchers have successfully boosted the mechanical properties of AMCs via the squeeze casting process [8].

Although the addition of reinforced particles improves the wear resistance and other mechanical properties of AMCs [9], the machining of such materials is difficult by traditional means [10, 11]. Reinforcement in AMCs has abrasive nature and retains a drastic threat to the tool life. Abrasion during machining erodes the tool material at a faster rate and causes early failure of the tool [12]. Moreover, reinforced particles are pulled out during machining and act as an abrasive cutting edge which deteriorates the surface finish of work material [13, 14]. For this reason, wire electric discharge machining (WEDM) has been observed as an attractive substitute for the machining of AMCs because of no physical contact between tool and workpiece. In this machining process, workpiece material is eradicated by the series of electric sparks between tool and workpiece [15, 16]. These electric sparks raise the temperature of the tool and workpiece interface up to 12000°C which melts and evaporates workpiece material [16]. A thin wire of molybdenum, tungsten, brass, or copper having a diameter of 0.05-0.3mm is typically used as a tool/electrode. Consequently, narrow kerfs are generated in the workpiece as compared to the conventional machining process which is also a perk of the WEDM process [17]. Dielectric fluid is generally used to maintain the insulating medium between electrode and workpiece. It also helps in flushing the eroded material from the machining zone due to high pressure [18]. Generally, the parts manufactured by composites or extremely hardened materials bearing intricate contours are machined precisely by the WEDM process with superior surface quality [19].

Keeping in view the demand in the manufacturing sector, researchers are focusing on the analysis of the working/machining behavior of hybrid AMCs due to their distinct properties. Therefore, several studies have been conducted to investigate the parametric effects on machining characteristics of various hybrid AMCs fabricated by different techniques. Muniappan et al., [20] described the effects of cutting parameters including V, I, $T_{ON}$, $T_{OFF}$, $T_{W,}$ and $F_R$ on the CS of Al6061/SiC/graphite hybrid AMC prepared by the stir casting process. $T_{OFF}$ followed by $T_{ON}$, V and I was observed as a significant parameter. Satishkumar and Kanthababu [21] compared the machined surface quality of simple Al7075 alloy and Al7075/$B_4C$/$Al_2O_3$ hybrid AMC fabricated by the stir casting process. It was noticed that simple Al7075 alloy at high $T_{OFF}$ and low $T_{ON}$ values generate comparatively less SR. Ugrasen et al., [22] investigated the influence of process parameters (I, $T_{ON}$, $T_{OFF}$, and bed speed) on the machining of Al2024/TiC/fly-ash hybrid AMC synthesized by stir casting technique. At lower values of $T_{OFF}$ and bed speed and higher values of I and $T_{ON}$, improved surface finish and dimensional accuracy were attained. Nag et al., [23] analyzed the impact of process parameters on the machining performance of A359/$Al_2O_3$/$B_4C$ hybrid

AMC produced by electromagnetic stir casting process. Analysis of the material removal rate and SR values showed $T_{ON}$ as the most significant input variable. Kumar et al., [24] employed Al6351/SiC/$B_4C$ hybrid AMC prepared by stir casting technique for the parametric optimization in the WEDM process. Their findings revealed that concentration of boron carbide particles has a significant impact on SR. Prakash et al., [25] examined the influence of V, $T_{ON}$, $T_{OFF}$, $F_R$, and concentration of two distinct reinforced particles on material removal rate of Al356/$B_4C$/fly-ash hybrid AMC manufactured by the stir casting process. Their results declared that V and $T_{ON}$ have considerable impact and concentration of reinforced particles has a negligible effect on material removal rate. Lal et al., [26] fabricated AA7075/SiC/$Al_2O_3$ hybrid AMC by inert gas-assisted electromagnetic stir casting technique to analyze the effects of input variables ($T_{ON}$, $T_{OFF}$, I, and $S_W$) on KW of AMC. From the literature, it has been observed that the machining performance of composites also depends upon the fabrication technique of the composite material [27]. Unfortunately, the machining of squeeze casted hybrid AMCs is scarcely reported.

To improve the machinability of hardened materials, cutting tools are treated cryogenically before machining. In cryogenic treatment, the material is kept at a very low temperature for a specific period resulting in improved electrical properties which are primarily imperative in electric discharge machining [28]. Superior electrical properties of electrode yield high material removal rate and surface finish [29]. Besides this, tool life and wear resistance of the alloys are also significantly enhanced with appropriate cryogenic treatment [30]. In this type of treatment, cooling time, soaking rate and temperature are the critical parameters that alter the properties of alloys [31-33]. Researchers have tried to optimize these parameters to achieve the desired material characteristics. Three particular sub-zero temperature ranges: (i) 223~193K (cold/cryogenic treatment), (ii) 193~113K (shallow cryogenic treatment) and (iii) 113~77K (deep cryogenic treatment) are mainly used for cryogenic treatment [34]. Tahir et al., [17] analyzed the effects of wire type (cold treated brass wire and non-cold treated brass wire) along with other input variables during machining HSLA steel. In wire type, cold treated brass wire yielded better surface finish and CS as compared to non-cold treated brass wire. Kapoor et al., [35] employed shallow cryogenic treated and non-treated brass wire for the machining of EN-31 steel. Their analysis indicates that shallow cryogenic treated wire has significantly reduced the SR. Kapoor et al., [36] compared the machining performance of non-cryogenic treated and deep cryogenic treated brass wire electrodes while cutting En-31 steel. Machining with deep cryogenic treated brass wire resulted in higher material removal rate than non-cryogenic treated brass wire. Nayak and Mahapatra [37] used deep cryogenic treated wire (Bronco cut-W wire) and workpiece material

(Inconel 718) to improve the machining performance evaluated by the results of angular error, SR, and CS. Goyal [38] investigated the effects of NT and CT wire in the machining of Inconel 625. In their results, CT wire offered better results for material removal rate and SR. Previous studies have presented the cryogenically treated electrodes as the best electrode alternative for the machining of hardened alloys. While machining of squeeze casted AMCs with cryogenically treated wire electrode is not adequately addressed in the literature.

From the comprehensive literature review, it has been reported that researchers have used AMCs prepared by various techniques in the WEDM process. However, there is a need to explore the machining of squeeze casted hybrid AMCs by the WEDM process. Owing to excessive hardness and high amount of reinforcement particulates, machining of squeeze casted AMCs resulted in high electrode wear and SR [39]. Therefore, this research has been conducted to determine the appropriate wire electrode for the precise machining of the Al2024/$Al_2O_3$/W squeeze casted hybrid composite. As the material is squeeze casted, so, it is also desired to identify the optimum set of input variables along with the selection of the best suitable wire type. For this reason, four input variables including pulse duration, wire tension, wire feed rate, and wire runoff speed have been used to analyze the effects of input variables on cutting speed, surface roughness, and kerf width. To investigate the appropriate wire type for the machining of Al2024/$Al_2O_3$/W, cryogenically treated moly wire, simple moly wire, cryogenic treated zinc-coated brass wire, and simple zinc-coated brass wire electrodes have been selected. Box Behnken design of RSM has been adopted for experimental design and ANOVA has been performed for analysis of the effects of input variables on response measures. For multi-objective optimization, grey relational analysis has been applied in this study.

# 2 Materials and methods

## 2.1 Fabrication of Al2024/$Al_2O_3$/W through squeeze casting technique

To analyze the effects of wire type and input variables on the machining performance of hybrid composite, Al2024/$Al_2O_3$/W has been fabricated by the squeeze casting process. The chemical composition of the matrix material used in the preparation of hybrid AMC has been given in Table 1. For the desired assortment of mechanical properties of composite, $Al_2O_3$ (3wt%) and W (1.5wt%) particles are used for the preparation of

hybrid AMC having an average particle size of 10 nm and 200 nm respectively. Squeeze casting setup used for the preparation of hybrid AMC specimens has been displayed in Fig. 1.

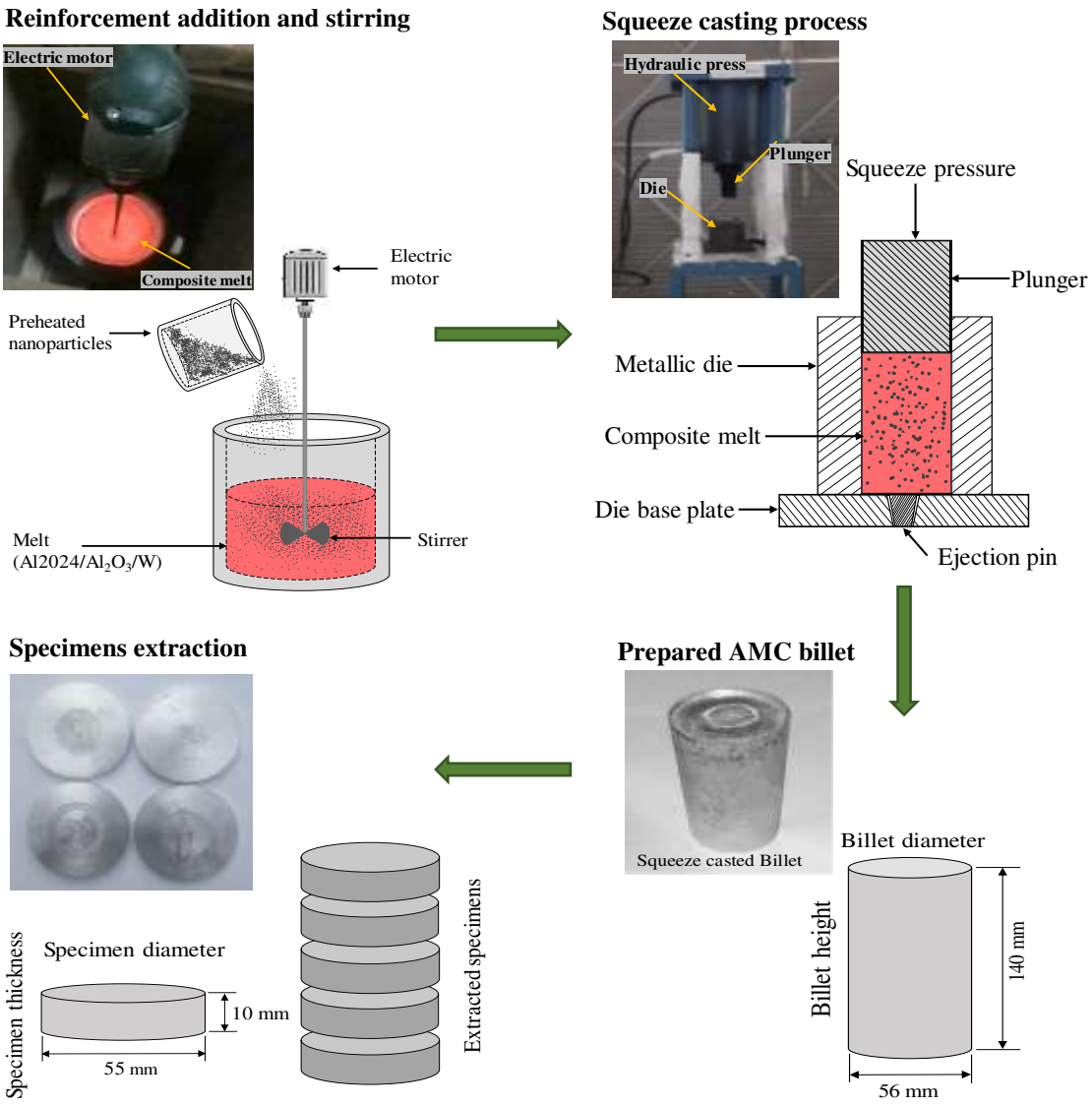


Figure 1. Hybrid AMC specimens' preparation through the squeeze casting process and its schematic illustration

Table 1. Chemical composition of matrix material (Al2024)

| Elements | Ti | Si | Ni | Mg | Cu | Mn | Al |
|---|---|---|---|---|---|---|---|
| Wt% | 0.02 | 0.15 | 0.03 | 1.21 | 3.84 | 0.60 | Balanced |

The setup used for the fabrication of AMC comprised of an electric furnace for the preparation of melt and preheating of alumina and tungsten particles, a mechanical stirrer for the uniform blending of $Al_2O_3$ and W particles in the melt, a metallic die in which a mixture of $Al_2O_3$ and W particles and melt is poured and a hydraulic press for the squeezing the composite melt. Melting of substrate metal (Al2024) was carried out in the electric

resistance furnace and its superheat was maintained at 825 °C. To improve the wettability of $Al_2O_3$ and W particles in the metal matrix, particles were preheated at 950 °C for 3 h in the separate furnace. For the uniform distribution of $Al_2O_3$ and W particles in the metal matrix, a double stirring mechanism was opted. A prepared mixture of melt, $Al_2O_3$, and W particles was poured into the preheated (225 °C) metallic die and kept under high pressure of 100 MPa for 2 min. A solidified billet of hybrid AMC having 56 mm diameter and 140 mm height was extracted from the metallic die. For WEDM experimentation, 10 mm thick slices were elicited from the cylindrical billet. The hardness of the specimens was determined by micro-Vickers hardness tester at a load of 0.5 kg for 20 s. The hardness of squeeze casted hybrid AMC was measured to be 165 HV. Due to the presence of nanoparticles and high squeeze pressure, the ultimate tensile strength (UTS) of fabricated hybrid AMC was also found exceptionally higher (441 MPa). To visualize the dispersion of nanoparticles throughout the metal matrix, SEM micrograph is shown in Fig. 2(a). It can be seen that nanoparticles are distributed uniformly throughout the metal matrix, however, some clusters may exist due to high squeeze pressure. Microstructure of the composite material has also been analyzed on a higher resolution to visualize the dispersion of smaller sized $Al_2O_3$ particles (Fig. 2b).

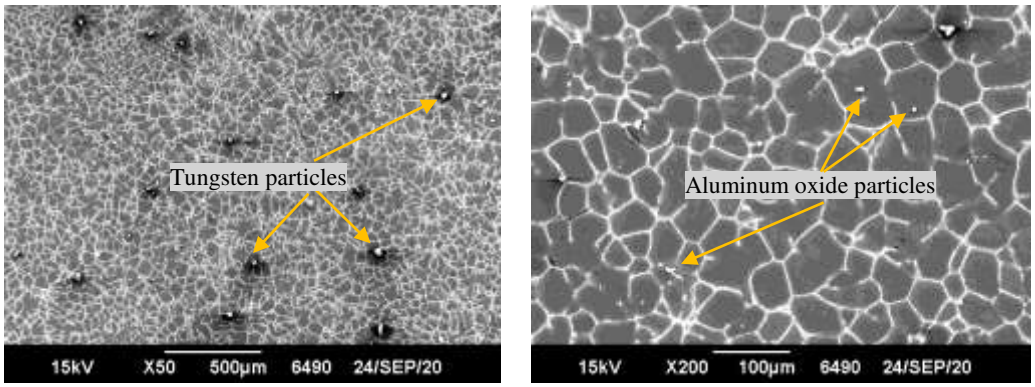


(a) (b)

Figure 2. Microstructure of squeeze casted composite material showing (a) large sized tungsten and (b) comparatively smaller sized $Al_2O_3$ nanoparticles shown at the higher resolution

## 2.2 Cryogenic treatment of wire electrodes

For the machining of the squeeze casted Al2024/$Al_2O_3$/W hybrid composite, two distinct wires including molybdenum and zinc-coated brass wires of diameter 0.3 mm have been selected. To enhance the electrical and mechanical properties, selected wires have been cryogenically treated using a temperature-controlled electrical chamber (CTT-SC-7520-02FI). Soaking of both wires has been performed at -70°C for 24h employing a ramp rate of 2°C/min. After cryogenic treatment, electrical conductivities of treated and non-treated wires have been tested on a portable Kelvin Bridge tester. UTS of selected wires has been measured on a universal testing machine

as per E8 ASTM standards. Results of electrical conductivity and UTS of tested wires are given in Table 2. It can be seen that UTS of molybdenum wire has increased to 1765 MPa while its electrical conductivity has been reduced from $2.08\times10^7$ to $2.02\times10^7$ S/m. In comparison with UTS, electrical conductivity is a fundamental property of the electrode for electric discharge machining. Reduced electrical conductivity of the electrode results in insufficient electrical spark density which effects the material removal process. This insufficient electrical conductivity declines CS and produces non-uniform and ineffective pulses which eventually generate poor surface finish [39]. Therefore, cryogenically treated molybdenum wire seems to be inappropriate for electric discharge machining hybrid AMC.

Table 2. Effect of cryogenic treatment on electrodes' properties

| Wire type | Electrical conductivity (S/m) | UTS (MPa) |
|---|---|---|
| Simple molybdenum wire | $2.08 \times 10^7$ | 1652 |
| Cryogenic treated molybdenum wire | $2.02 \times 10^7$ | 1765 |
| Zinc coated brass wire | $12.5 \times 10^6$ | 686 |
| Cryogenic treated zinc-coated brass wire | $15.6 \times 10^6$ | 727 |

On the other hand, the UTS of zinc-coated brass wire has been slightly decreased from 727 to 686 MPa. However, the electrical conductivity of cryogenic treated zinc-coated brass wire has been raised up to $15.6 \times 10^6$ S/m with a percentage increment of 24.8%. Therefore, zinc-coated brass wires have been observed as an attractive option for machining. A framework has been developed for the selection of the best suitable wire electrode for the machining of the squeeze casted Al2024/$Al_2O_3$/W hybrid composite shown in Fig. 3. The machining performance of the wire electrode has been analyzed on the basis of CS, SR, and KW. Keeping wires' treatment results in view, cryogenic treated zinc-coated brass wire has been selected for the machining of composite material.


Figure 3. Framework for the selection of appropriate wire electrode for the machining of the squeeze casted Al2024/$Al_2O_3$/W hybrid composite

To have a deeper insight into the effects of cryogenic treatment, the microstructure of simple zinc-coated and cryogenic treated wires has been analyzed on a scanning electron microscope (SEM). The micrograph of NT wire reveals the presence of microcavities and pores in its structure (Fig. 4a). These microcavities offer hindrance in the flow of electrons which declines thermal and electrical conductivity. While the cryogenic treatment has increased the soundness and stability by reducing micro-cavities can be seen in Fig. 4b. As temperature decreases, atomic bonding in brass start to abate, and crystal structure regress towards its original phase. Residual stresses in the brass wire structure are also minimized in cryogenic treatment [40]. Machining with CT wire depicts the

intense electric discharge in the machining zone due to improved thermal and electrical conductivity as compare to NT wire. The same phenomenon of the machining of AMC with NT and CT wires are shown in Fig. 5a-b.

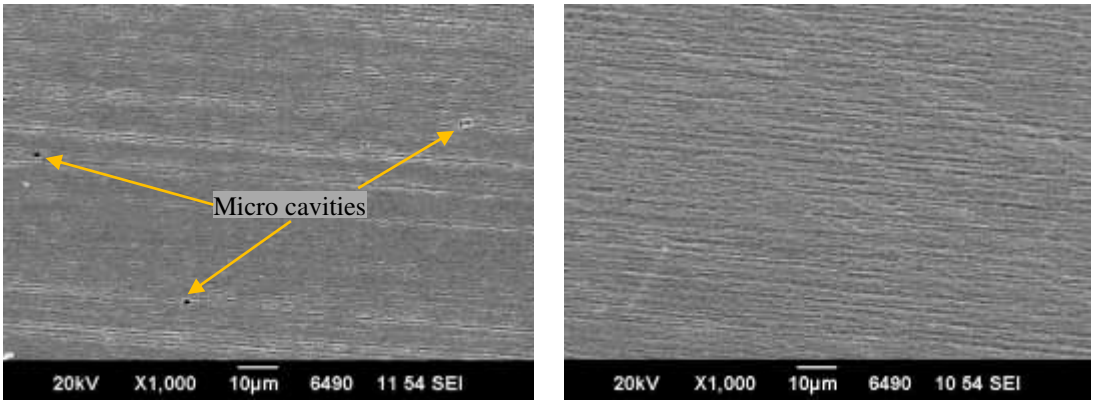


(a) (b)

Figure 4. Microstructure of (a) non-treated and (b) cryogenically treated brass wire

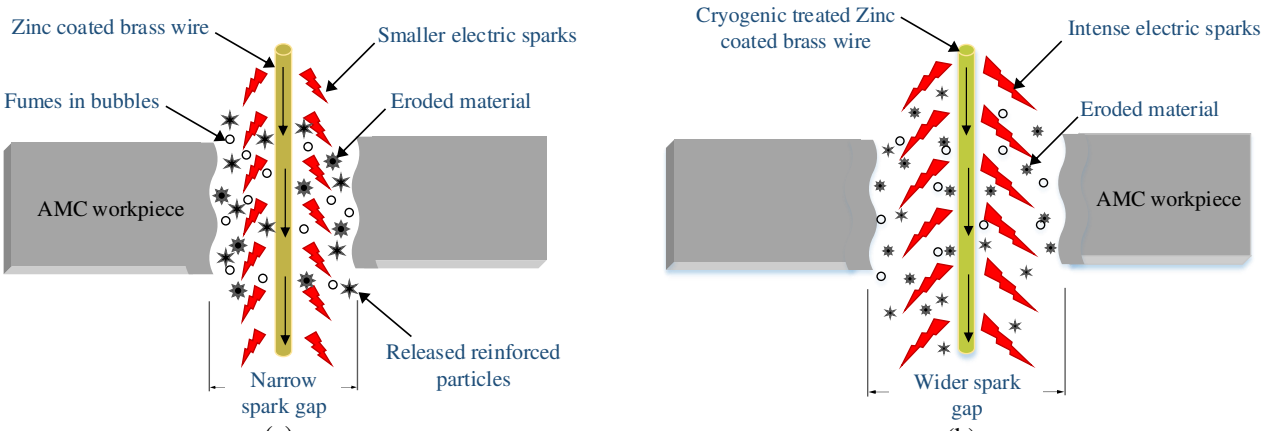


(a) (b)

Figure 5. Schematic illustration of the machining of AMC with (a) simple zinc coated brass wire (b) cryogenic treated zinc coated brass wire

## 2.3 Experimentation details

To investigate the effects of wire type and input variables on the machining of hybrid AMC a series of experiments has been conducted on WEDM. In wire type, cryogenic treated and simple zinc-coated brass wires have been selected for experimentation. Besides wire type, effects of input variables including pulse duration, wire tension, wire feed rate, and wire runoff speed on cutting speed, surface roughness, and kerf width have also been analyzed. Pilot experimentation has been conducted to explore the appropriate ranges of input variables for machining of Al2024/$Al_2O_3$/W hybrid composite. Selected ranges of input variables have been given in Table 3. Machining conditions other than input variables are provided in Table 4. For each experiment, CS has been determined by recording the cutting time of a predetermined cutting length of 27 mm. CS values obtained from the control unit

of the machine has been used to verify the calculated values of CS. SR of the cutting specimens has been measured using surface roughness tester (SJ-410). A coordinate measuring machine (CE-450DV) of 0.001 mm resolution has been employed for the measurement of KW. Surface morphology of wire and machined surfaces of workpiece has been analyzed on SEM (VEGA3) facility. The methodology of this research starting from machining to response measurement is shown in Fig. 6.

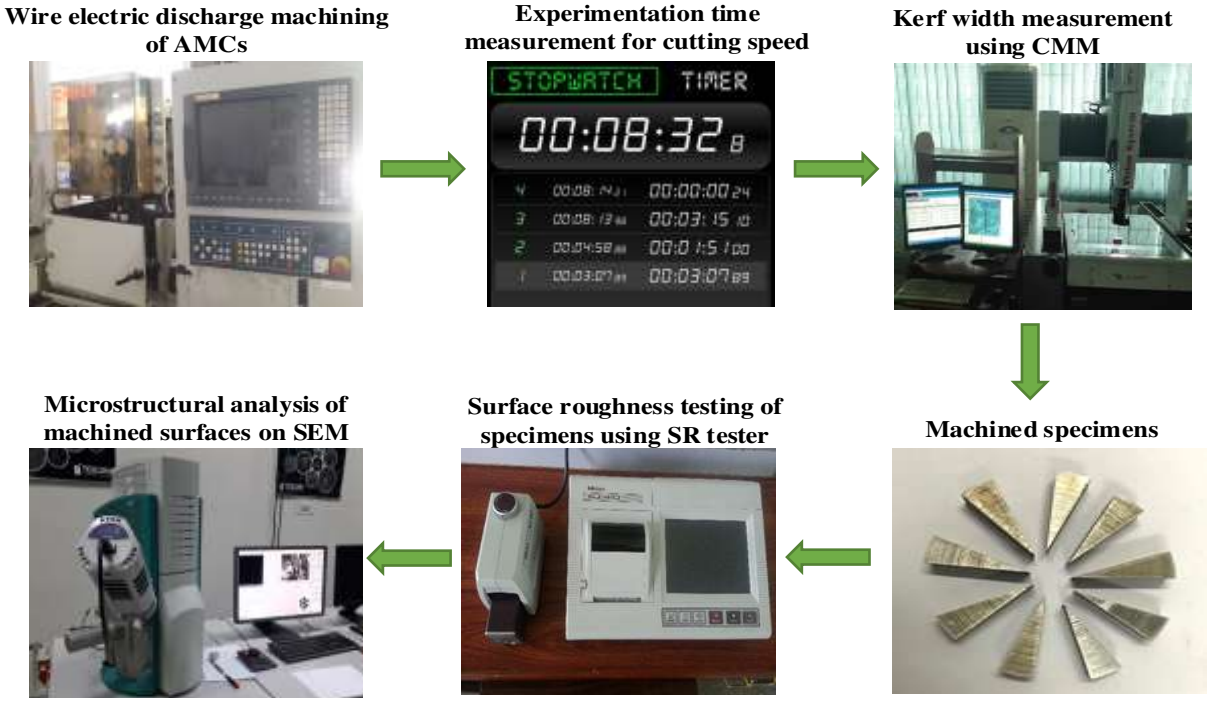


Figure 6. Experimental procedure and response measurement

Table 3. Description of input variables and their selected ranges

| Input variables | Description | Ranges |
|---|---|---|
| Pulse duration | the time interval in which discharge is produced | 1-5 µs |
| Wire feed rate | the rate at which wire passes through the guided path in a transverse direction | 10-16 m/min |
| Wire runoff speed | wire velocity along its longitudinal direction | 8-12 m/min |
| Wire tension | mechanical stress maintained in the wire | 4-10 g |

Table 4. Constant machining conditions

| Machining conditions | Description |
|---|---|
| Gap voltage | 45 V |
| Pulse off time | 26 µs |
| Servo voltage | 48 V |
| Flushing pressure (kg/cm²) | 4.5 |
| Dielectric fluid | Water mixed resin MBQR400 (ratio 30:1) |

## 2.4 Experimental design

### 2.4.1 Response surface methodology

In previous studies, numerous statistical techniques including Factorial design [41], Taguchi method [42], Response surface methodology [43], Genetic algorithm [44], Fuzzy logic [45], and Artificial neural network [46]

have been practiced for the design of experiments, analysis, empirical modeling, and optimization. In all types of designed experiments, there exist some variations in experimental results. However, RSM repeats some basic experiments known as center point experiments to minimize these variations. Replication of experiments enables the researcher to identify and reduce the experimental error. It also increases the precision and presents a more precise estimation of response variables in mathematical modeling. Moreover, RSM has distinctive capabilities of generating a reduced number of experiments for the development of empirical models with great accuracy, hence, RSM is regarded as the most effective approach for analysis [47]. RSM is normally adopted to investigate the nature of the relationship between input variables and response measures. RSM describes this relationship as follows:

$$R = f(T_{ON}, F_R, S_w, T_w) \quad (1)$$

where R is the response measure, f is the response surface, and $T_{ON}$, $F_R$, $S_w$, and $T_W$ are the input variables. Depending upon the nature of their relationship, RSM can use the second-order polynomial function for the empirical modeling due to its capability of analyzing the interaction effects of multiple variables. The quadratic regression model of R is exemplified below:

$$R = a_o + \sum_{i=1}^{4} a_i B_i + \sum_{i<j}^{4} a_{ij} B_i B_j + \sum_{i=1}^{4} a_{ii} B_i^2 \quad (2)$$

where $a_o$, $a_i$, $a_{ij}$, and $a_{ii}$ are the coefficients of constant, linear, interaction, and quadratic terms respectively.

Box Behnken design of RSM has been used for the design of experiments in this study. The design offers 30 number of experiments with 4 input variables. The complete design has been repeated for both cryogenic treated and simple zinc-coated brass wires separately, therefore, a total of 60 experiments have been conducted in this research. Results of CS, SR, and KW against each set of input variables for both wires are given in Table 5.

Table 5. Design matrix with measured response values

| Exp. No. | Input variables | | | | Response measures | | | | | |
|---|---|---|---|---|---|---|---|---|---|---|
| | | | | | Zinc coated brass wire | | | Cryogenic treated zinc-coated brass wire | | |
| | Pulse duration ($T_{ON}$) | Wire feed rate ($F_R$) | Wire runoff speed ($S_W$) | Wire tension ($T_W$) | Cutting speed | Surface roughness | Kerf width | Cutting speed | Surface roughness | Kerf width |
| | µs | m/min | m/min | g | mm/min | µm | mm | mm/min | µm | mm |
| 1 | 1 | 10 | 8 | 7 | 1.88 | 2.35 | 0.401 | 2.05 | 1.95 | 0.443 |
| 2 | 5 | 10 | 8 | 7 | 5.13 | 3.01 | 0.429 | 6.21 | 2.57 | 0.471 |
| 3 | 1 | 16 | 8 | 7 | 3.07 | 2.59 | 0.349 | 3.67 | 2.21 | 0.354 |
| 4 | 5 | 16 | 8 | 7 | 7.16 | 3.84 | 0.409 | 9.09 | 3.12 | 0.440 |
| 5 | 3 | 13 | 5 | 4 | 2.30 | 2.39 | 0.398 | 2.73 | 1.98 | 0.437 |
| 6 | 3 | 13 | 11 | 4 | 3.16 | 2.75 | 0.384 | 3.74 | 2.09 | 0.421 |
| 7 | 3 | 13 | 5 | 10 | 2.92 | 2.29 | 0.368 | 3.13 | 1.42 | 0.405 |
| 8 | 3 | 13 | 11 | 10 | 3.83 | 2.15 | 0.318 | 5.37 | 1.82 | 0.340 |
| 9 | 1 | 13 | 8 | 4 | 1.84 | 2.19 | 0.395 | 1.86 | 1.84 | 0.425 |

| | | | | | | | | | | |
|---|---|---|---|---|---|---|---|---|---|---|
| 10 | 5 | 13 | 8 | 4 | 5.15 | 3.48 | 0.422 | 5.93 | 2.98 | 0.439 |
| 11 | 1 | 13 | 8 | 10 | 2.20 | 2.23 | 0.342 | 2.35 | 1.89 | 0.355 |
| 12 | 5 | 13 | 8 | 10 | 6.05 | 2.91 | 0.399 | 7.53 | 2.33 | 0.429 |
| 13 | 3 | 10 | 5 | 7 | 2.82 | 1.92 | 0.405 | 3.60 | 1.63 | 0.447 |
| 14 | 3 | 16 | 5 | 7 | 4.40 | 2.34 | 0.377 | 5.72 | 2.02 | 0.413 |
| 15 | 3 | 10 | 11 | 7 | 3.65 | 2.10 | 0.387 | 4.67 | 1.81 | 0.426 |
| 16 | 3 | 16 | 11 | 7 | 5.15 | 2.72 | 0.358 | 6.68 | 2.33 | 0.391 |
| 17 | 1 | 13 | 5 | 7 | 1.76 | 2.01 | 0.393 | 1.94 | 1.57 | 0.433 |
| 18 | 5 | 13 | 5 | 7 | 4.89 | 2.93 | 0.430 | 5.94 | 2.36 | 0.472 |
| 19 | 1 | 13 | 11 | 7 | 2.32 | 2.19 | 0.374 | 2.67 | 1.73 | 0.412 |
| 20 | 5 | 13 | 11 | 7 | 6.37 | 3.19 | 0.409 | 7.84 | 2.59 | 0.451 |
| 21 | 3 | 10 | 8 | 4 | 2.41 | 2.31 | 0.408 | 2.73 | 1.99 | 0.459 |
| 22 | 3 | 16 | 8 | 4 | 3.97 | 3.00 | 0.376 | 4.82 | 2.58 | 0.397 |
| 23 | 3 | 10 | 8 | 10 | 2.98 | 2.17 | 0.372 | 3.46 | 1.85 | 0.388 |
| 24 | 3 | 16 | 8 | 10 | 4.71 | 2.71 | 0.346 | 5.76 | 2.33 | 0.377 |
| 25 | 3 | 13 | 8 | 7 | 3.68 | 2.38 | 0.376 | 4.05 | 1.89 | 0.404 |
| 26 | 3 | 13 | 8 | 7 | 3.92 | 2.31 | 0.379 | 4.30 | 1.83 | 0.407 |
| 27 | 3 | 13 | 8 | 7 | 3.57 | 2.46 | 0.382 | 3.84 | 1.96 | 0.412 |
| 28 | 3 | 13 | 8 | 7 | 3.65 | 2.38 | 0.375 | 4.14 | 1.89 | 0.403 |
| 29 | 3 | 13 | 8 | 7 | 3.74 | 2.51 | 0.371 | 4.22 | 1.92 | 0.398 |
| 30 | 3 | 13 | 8 | 7 | 3.61 | 2.47 | 0.388 | 4.06 | 1.97 | 0.417 |

# 3 Results and discussions

This section covers the analysis of response measures by ANOVA, empirical modeling of individual response measures, analysis of the effects of input variables using 3D response surface graphs, microstructural analysis, multi-objective optimization using GRA, and performance comparison of NT and CT wire electrodes.

## 3.1 Main and interaction effects analysis

The effects of input variables on the response measures are presented in the form of 3D response surface graphs. The 3D surface of the graph depicts the main as well as the interaction effects of two input variables simultaneously while keeping other variables constant at their mid-levels [48]. Contour lines on the base of the graph depict the reflection of 3D surface. Contour lines with distinct colors present the response values range from minimum to maximum.

### 3.1.1 Cutting speed

The effects of $F_R$, $T_{ON}$, $T_{W,}$ and $S_W$ on the CS for both NT and CT wires are shown in Fig. 7a-d. It has been observed that CS increases with an increment in both $T_{ON}$ and $F_R$ (Fig. 7a-b). The value of CS is smaller at the lower level of $T_{ON}$ as discharge energy is provided for a shorter time span which enables the reinforced particles to protect the metal matrix from melting with their strong bonding. With an increase in $T_{ON}$, the discharge energy is supplied for more time to eradicate material from the work surface. This intense discharge energy melts and evaporates aluminum matrix easily and release the reinforced particles, this is the reason that a slight increase in $T_{ON}$ raises the CS promptly. Similar trends of $T_{ON}$ has been reported by Kavimani et al., [49]. High CS has been

observed at a higher level of $F_R$. As the increase in $F_R$ value raises the chance of new wire to expose and create clear and higher intensity sparks. This intense spark energy is responsible for material erosion by broadening and deepening the cutting zone [50].

Fig. 7c-d shows the effects of $S_W$ and $T_W$ on CS. It has been noticed that CS enhances by an increase in $S_W$ with a nonlinear trend. As increment in $S_W$ increases the rate of spark discharge which leads to the high amount of heat energy delivered to the cutting zone ultimately enhances the rate of melting and evaporation of work material [51]. From Fig. 7c-d, it has been observed that increase in $T_W$ improves the CS of composite material due to increased straightness of wire. While low CS has been reported at lower $T_W$ because wire vibrates and lags behind during cutting [52]. Within the suitable range of $T_W$, CS increases with $T_W$.

Comparatively analysis of the performance of both wire electrodes in Fig. 7 shows that CS of CT wire is high during the cutting of squeeze casted hybrid AMC. As in cryogenic treatment, the crystal structure of the electrode gets refines and makes the electron flow uniform and easier. The absence of any obstacles in the structure of electrode material enhances the electron flow per unit time which improves the electrical conductivity of the cryogenically treated material. Owing to the high electrical conductivity of cryogenically treated brass wire, a high amount of energy is supplied to the machining zone which melts and evaporates matrix material at a faster rate. Intense sparking is produced removes more material from the machining zone and the same phenomenon can be observed in Fig. 4b. It releases the reinforced particles from the matrix swiftly which increases the material removal rate and ultimately enhances the CS.

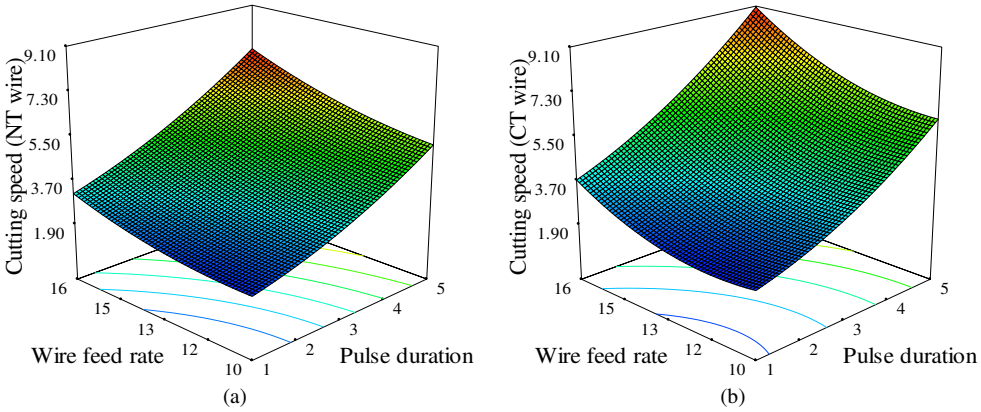

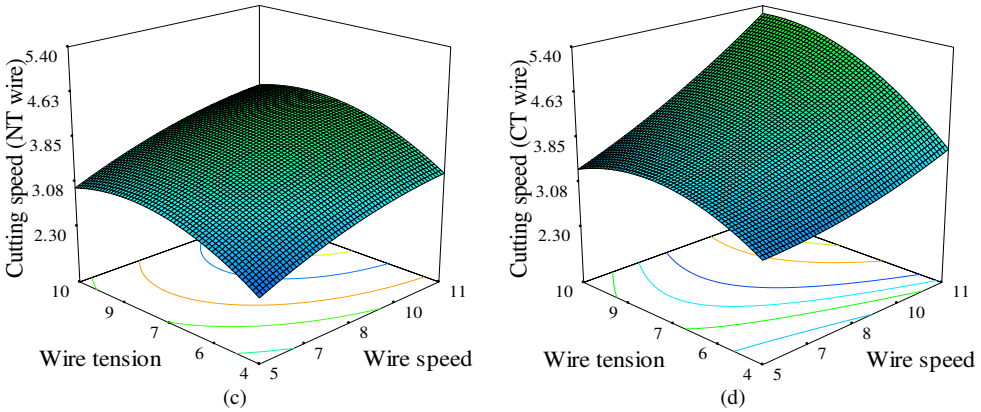


Figure 7. 3D response surface graphs presenting the effects of $T_{ON}$ and $F_R$ on CS for (a) NT wire (b) CT wire and $S_W$ and $T_W$ on CS for (c) NT wire and (d) CT wire

### 3.1.2 Surface roughness

Surface graphs for NT and CT wires presenting the effects of input variables on SR are shown in Fig. 8a-d. It is cleared from Fig. 8a-b that SR is maximum at a higher level of Ton and $F_R$. Increase in feed rate, the wire gets renewed and recovered hastily during machining. This introduction of non-worn fresh wire apparently enhances the sparking efficiency which creates larger and deeper craters [50]. While the increase in $T_{ON}$ increases the time duration of electric discharges which melts more workpiece and produces large-sized craters. These large-sized craters create irregularities on the machined surface eventually increase the SR [53].

Fig. 8c-d depicts the effects of $S_W$ and $T_W$ on SR for both NT and CT wires respectively. It has been observed that SR rises initially then starts decreasing with an increase in $S_W$. Increase in $S_W$ allows the molten material to splash on the work surface with the flushing pressure and micro-voids are created due to the entrapment of gases. As a result of micro-voids in the molten pool high SR is originated [54]. On the other hand, SR declines with an increase in $T_W$ which is actually due to the decrease in wire amplitude at higher tension. Due to high $T_W$, the wire gets straightened and fluid begins to flow with higher speed around the wire which prevents the debris from adherence and keeps the workpiece surface clean. This ablution of the surface is responsible for low SR at higher $T_W$ [52].

From response surface graphs in Fig. 8, it has been observed that CT wire yields less SR as compared to NT wire. As earlier discussion shows that CT wire has high electrical conductivity, which is also responsible for the reduction in SR. Because higher electrical conductivity of the electrode widens the discharge channel resulting in easier flushing of debris and released reinforced particles from the machining zone and keeps the machined surface cleaner. Moreover, this enlarged discharged channel distributes the spark energy uniformly in all

orientations which produce small and uniform sized craters on the machined surface as compare to NT wire and the same behavior of CT wire can be realized in Fig. 5a-b. Therefore, CT wire results in superior surface quality for composite material.

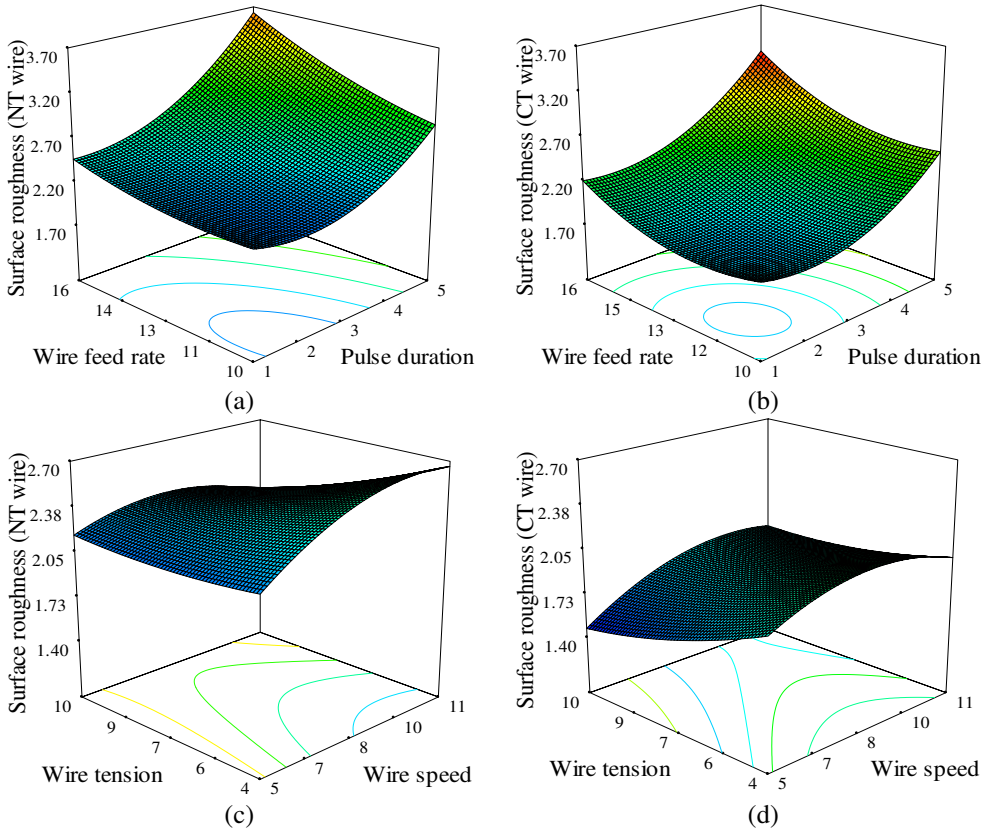


Figure 8. 3D response surface graph for the effects of $T_{ON}$ and $F_R$ on SR for (a) NT wire (b) CT wire and $S_W$ and $T_W$ on SR for (c) NT wire and (d) CT wire

### 3.1.3 Kerf width

KW is the gap created as a result of the cutting process that increases or decreases with variation in machining parameters. Change in KW with variation in input variables are presented in Fig. 9a-d. In this study, it has been observed that KW of hybrid AMC reduces with decrease in $F_R$ and increase in Ton (Fig. 9a-b). However, $T_{ON}$ has a significant impact on KW as compared to $F_R$. As the increase in $T_{ON}$ offers more time to discharge energy for melting and vaporizing the work material. At a low level of $T_{ON}$, discharge energy is not sufficient to remove work material easily, while at higher values of $T_{ON}$, intense discharge energy melts the substrate metal and break the $Al_2O_3$ and W particles' bound from the matrix. Thus removal of reinforcement particles increases the KW significantly [24]. It has been observed that an increase in $F_R$ decreases the KW because a higher feed rate does

not let the wire electrode to distribute heat energy uniformly in the cutting zone. Therefore, the ineffective distribution of heat energy in the machining zone results in reduced KW [55].

From Fig. 9c-d, it can be clearly seen that KW is minimum at higher values of $T_W$ and $S_W$. When $S_W$ is low, the amplitude of wire vibration is comparatively higher which reduces the dielectric fluid flow around the wire and resulted in inefficient eradication of debris and reinforced particles from the discharge gap. Moreover, the debris particles which adhered around the wire also generate high KW. When the wire is running at a higher speed the debris and reinforced particles get discarded from the wire surface and resulted in reduced KW [56]. From the 3D surface graph, it can be seen that KW decreases as tension in the wire increases. At low $T_W$, the amplitude of the wire is comparatively high resulted in the wider kerf. Average vibration amplitude decreases with an increase in $T_W$ which ultimately yields narrow KW [57].

From Fig. 9 it has been observed that CT wire generated wider kerf than NT wire in AMC. This increase in kerf is due to the higher electrical conductivity of CT wire. The high electrical conductivity of the electrode produces intense discharge energy to the machining zone and removes a high amount of composite material. Improved flushing using CT wire prevents debris and residue material from adherence and keeps the spark gap cleaner. Moreover, the melting of matrix material releases the large-sized reinforced particles from the machining zone which also increases the spark gap abruptly. The actual phenomenon of the widening of spark gap is illustrated in Fig. 5 schematically. This increase in spark gap resulted in high kerf width of composite material with CT wire.

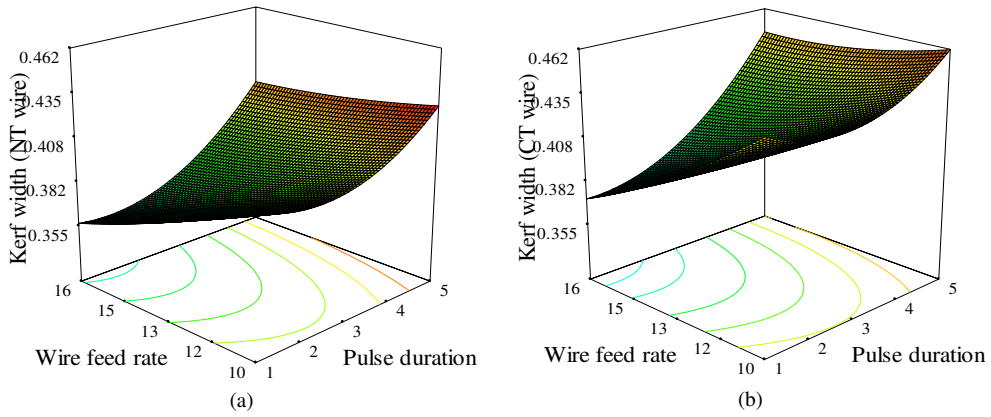

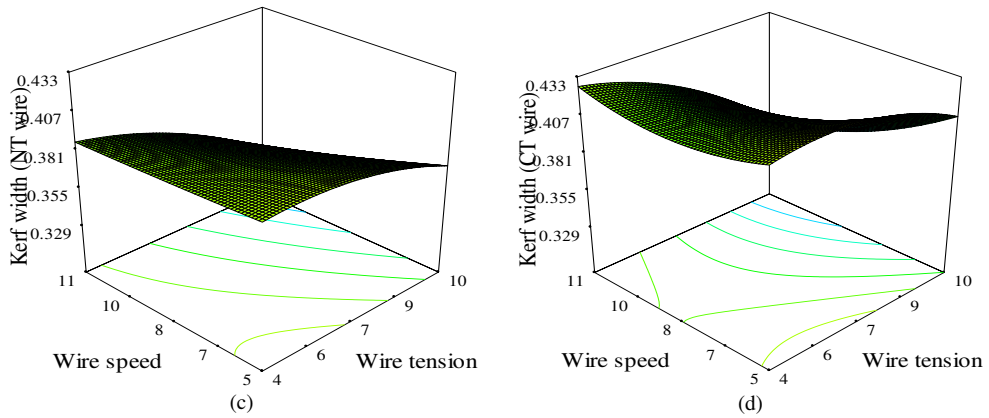


Figure 9. 3D response surface graph showing the influence of $T_{ON}$ and $F_R$ on KW for (a) NT wire (b) CT wire and $S_W$ and $T_W$ on KW for (c) NT wire and (d) CT wire

## 3.2 Microstructural analysis

### 3.2.1 Surface morphology of workpiece

The surface morphology of the machined specimens has been analyzed using SEM shown in Fig. 10a-d. To clearly visualize the effects of input variables and cryogenic treatment of the wire electrode, the surface morphology of specimens machined with NT and CT wires has been compared. For this aspiration, specimens bearing minimum and maximum SR values are analyzed at Exp. No. 13 and 04 respectively are provided in Table 5 for both wire electrodes. Better surface morphologies of NT (1.92 µm) and CT wire (1.63 µm) have been seen at $T_{ON}$=3 µs, $F_R$=10 m/min, $S_W$=5 m/min, and $T_W$=7 g displayed in Fig 10a-b respectively. On the other side, Fig. 10c-d display deprived surfaces of machined specimens (3.84 µm 3.12 for NT and CT wire respectively) at $T_{ON}$=5 µs, $F_R$=16 m/min, $S_W$=8 m/min, and $T_W$=7 g. From the above comparison, it has been seen that NT wire results in inferior surface morphology than CT wire in both cases. Surface morphology of specimens machined with NT wire depicts micro-voids, globules, and large craters while CT wire resulted in small and shallow sized craters and few debris particles welded on the surface have also been noticed. The reason behind the remarkable performance of CT wire is the enlarged discharge channel which prevents the melted material from resolidification on the work surface and makes the flushing easy due to its superior electrical conductivity.

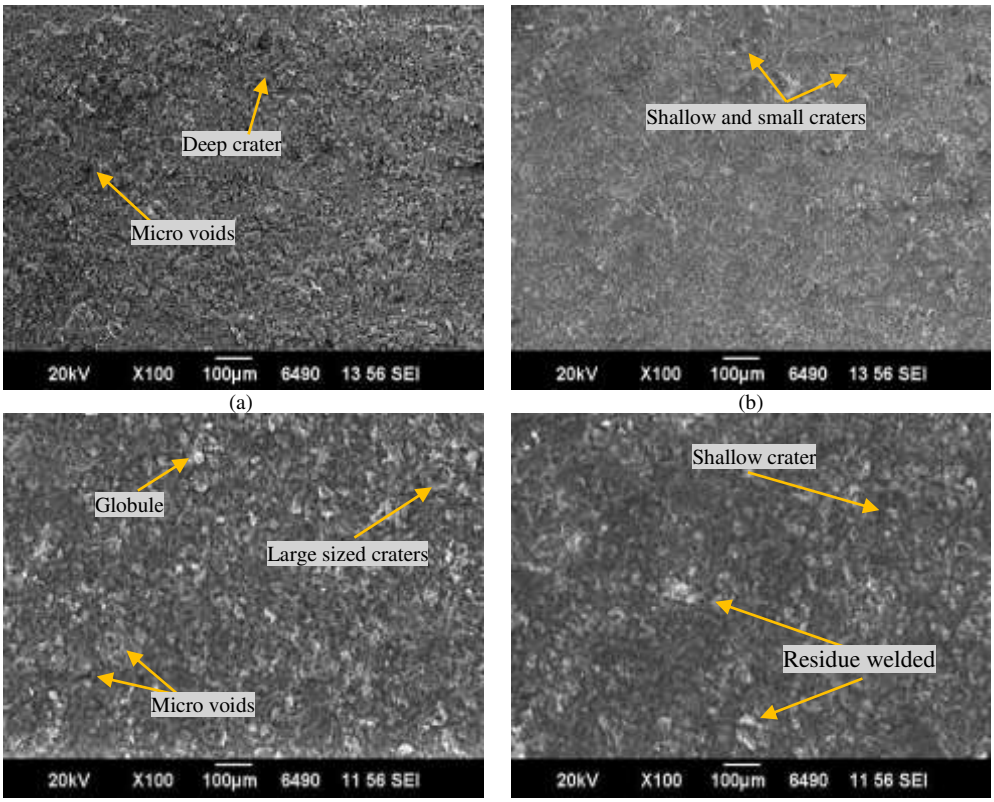


Figure 10. Microstructure of the machined surfaces at Exp. No. 13 for (a) NT (b) CT wires and Exp. No. 04 for (c) NT (d) CT wires

### 3.2.2 Kerf width

To visualize the difference in the performance of NT and CT wire electrodes, micrographs at lower and higher values of KW have been compared. For this purpose, the KW of both wires has been analyzed at Exp. No. 08 and 18 showing the minimum and maximum values are presented in Table 5. From Fig. 11a-b, it can be observed that low energy parameters ($T_{ON}$=3 µs, $F_R$=13 m/min, $S_W$=11 m/min, and $T_W$=10 g) at Exp. No. 08 has generated narrow kerf. When the comparison has been made between Fig. 11a and 11b, it can be seen that CT wire has produced a relatively higher KW value (0.340 mm) than NT wire (0.318 mm). However, high energy parameters $T_{ON}$=5 µs, $F_R$=13 m/min, $S_W$=5 m/min, and $T_W$=7 g at Exp No. 18 have resulted in wider kerfs 0.430 mm and 0.472 mm for NT and CT wires respectively. High energy parameters result in high explosions and intense sparking which ultimately produce large-sized kerf. In comparison with CT wire, NT wire has produced narrow KW due to poor flushing and allows the debris material to re-solidify on the machined surface and the same phenomenon can be observed in Fig. 11c-d.

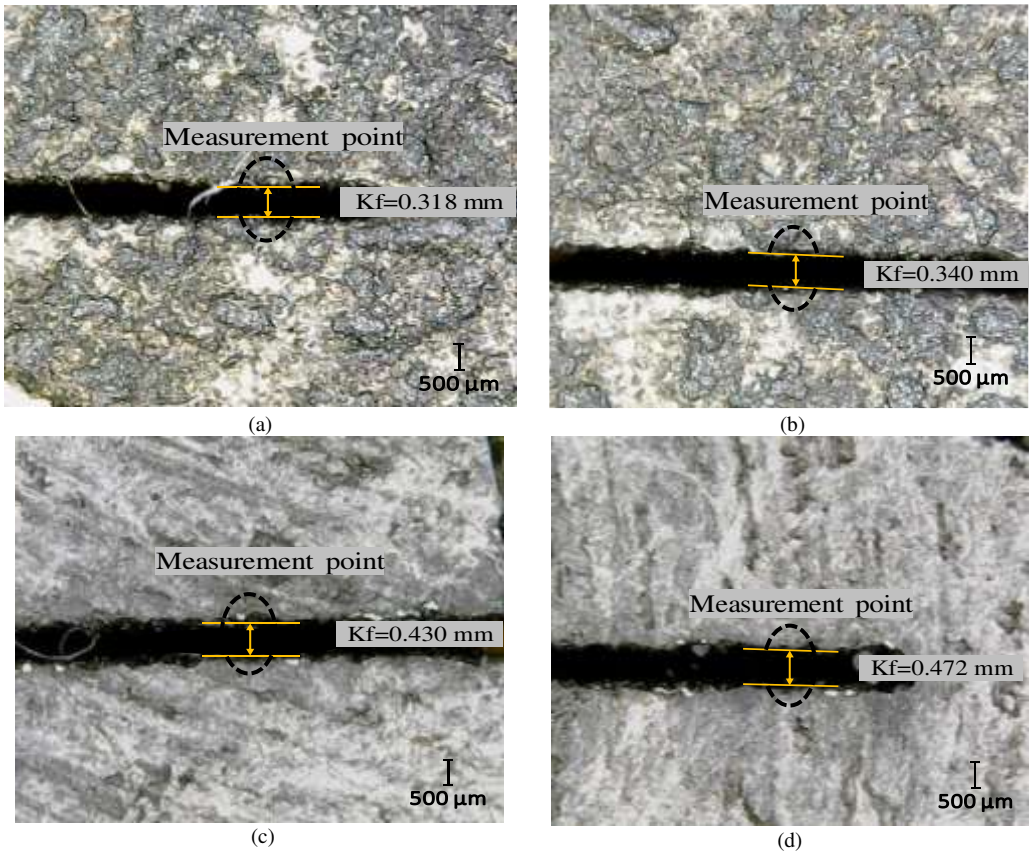


Figure 11. Micrograph showing minimum KW values at Exp. No. 08 using (a) NT wire, (b) CT wire, and maximum KW values at Exp. No. 18 with (c) NT wire and (d) CT wire

### 3.2.3 Wire surface analysis

In the machining of squeeze casted hybrid composite, the effects of wire's cryogenic treatment and machining variables have also been analyzed on wire surface. For this mean, micrographs of NT and CT wire have been compared at Exp. No. 04. In Fig. 12, the surface integrity of both wires shows the difference in erosion patterns during the machining of squeeze casted hybrid composite. Micrograph of eroded NT wire in Fig. 12(a) depicts some micro-cracks and clusters of voids on its surface. Besides this, larger and deeper craters have also been observed on its surface after machining. On the other hand, a shallow and small-sized crater has been seen on the CT wire's surface (Fig. 12b). At the same cutting conditions (Exp. No. 04) wear performance of wires shows that NT wire degenerates more swiftly as compared to CT. During machining, high temperature in the machining zone decreases the thermal conductivity of the wire electrode which melts and evaporates wire material and deteriorates the wire structure. Depreciation in wear behavior of CT wire is certainly due to the enhanced thermal and electrical conductivity attained during cryogenic treatment ultimately results in a comparatively smooth wire surface [58].

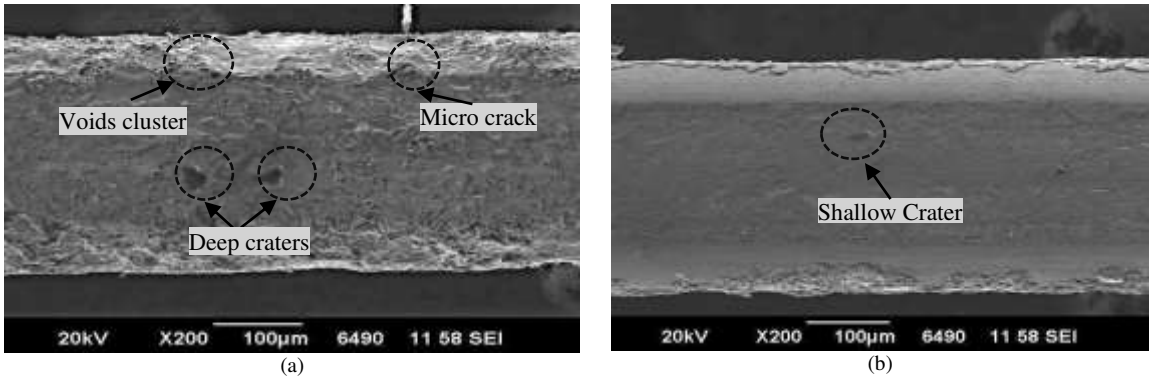


(a) (b)

Figure 12. Microstructure of (a) NT and (b) CT wire after experimentation

## 3.3 Analysis of variance

To analyze the effects of input variables, the design of experiment has been formulated using a statistical technique. Each technique involves randomization as a basic principle in experimental design. These techniques randomly allocate the experimental units as well as conducts experiments randomly. This randomization avoids biases in the conclusions for input variables. After designing the experiment, results are analyzed with Analysis of variance (ANOVA). ANOVA distributes the total variation into accountable sources of variations (input variables) in the experiments [59]. ANOVA also estimates the percentage contribution of input variables and their interactions into the corresponding response measures. To predict the response measures, empirical models for each response measure have been developed using experimental results. Statistical significance of developed empirical models, main, interaction, and quadratic terms has also been assessed in this study [60]. The coefficient of determination ($R^2$) ascertains the linear correlation of variables and response measures in the regression analysis and its higher values depict the adequacy of developed empirical models [61]. An adequate empirical model has the ability to predict the response measures with great accuracy.

### 3.3.1 Cutting speed

ANOVA of the CS results for both NT and CT wire electrodes have been provided in Table 6. Fit summary shows that all input variables have a significant impact on CS for both electrodes using 95% confidence level. The analysis shows that empirical models of CS for both wire electrodes are significant and adequacy measures ($R^2$, adjusted $R^2$, and predicted $R^2$) are also in reasonable agreement. This reveals that developed models for CS can predict response values with fine accuracy. Developed empirical models for NT and CT wires are presented in Eqs. 3 and 4 respectively.

$$\text{Cutting speed (NT wire)} = 1.965 - 0.575 \times T_{ON} - 0.762 \times F_R + 0.336 \times S_w + 0.611 \times T_W + (0.034 \times T_{ON} \times F_R) + (0.038 \times T_{ON} \times S_w) + (0.022 \times T_{ON} \times T_W) - (2.50 \times 10^{-3} \times F_R \times S_w) + (4.75 \times 10^{-3} \times F_R \times T_W) + (1.25 \times S_w \times T_W) + (0.093 \times {T_{ON}}^2) + (0.035 \times {F_R}^2) - (0.017 \times {S_w}^2) - (0.045 \times {T_W}^2) \quad (3)$$

$$\text{Cutting speed (CT wire)} = 12.204 - 1.019 \times T_{ON} - 1.819 \times F_R + 0.375 \times S_w + 0.348 \times T_W + (0.052 \times T_{ON} \times F_R) + (0.048 \times T_{ON} \times S_w) + (0.046 \times T_{ON} \times T_W) - (3.19 \times 10^{-3} \times F_R \times S_w) + (6.06 \times 10^{-3} \times F_R \times T_W) + (0.034 \times S_w \times T_W) + (0.130 \times {T_{ON}}^2) + (0.077 \times {F_R}^2) - (0.015 \times {S_w}^2) - (0.048 \times {T_W}^2) \quad (4)$$

### 3.3.2 Surface roughness

ANOVA results in Table 6 explain that empirical models of SR for NT and CT wire electrodes are significant as their probability values are less than 0.05. It is also observed that all input variables have also a significant effect on SR. Adequacy measures have also been focused during the analysis to check the adequacy of empirical models. Numerical values all coefficients are closer to 1 which shows the competitive prediction capabilities of developed SR models for both wires are presented in Eqs. 5 and 6.

$$\text{Surface roughness (NT wire)} = 2.168 - 0.425 \times T_{ON} - 0.285 \times F_R + 0.334 \times S_w + 0.132 \times T_W + (0.024 \times T_{ON} \times F_R) + (3.06 \times 10^{-3} \times T_{ON} \times S_w) - (0.024 \times T_{ON} \times T_W) + (5.59 \times 10^{-3} \times F_R \times S_w) - (4.15 \times 10^{-3} \times F_R \times T_W) - (0.013 \times S_w \times T_W) + (0.083 \times {T_{ON}}^2) + (0.011 \times {F_R}^2) - (0.017 \times {S_w}^2) + (4.31 \times 10^{-3} \times {T_W}^2) \quad (5)$$

$$\text{Surface roughness (CT wire)} = 4.789 - 0.241 \times T_{ON} - 0.598 \times F_R + 0.213 \times S_w - 0.074 \times T_W + (0.011 \times T_{ON} \times F_R) + (2.62 \times 10^{-3} \times T_{ON} \times S_w) - (0.029 \times T_{ON} \times T_W) + (3.69 \times 10^{-3} \times F_R \times S_w) - (3.27 \times 10^{-3} \times F_R \times T_W) + (8.07 \times 10^{-3} \times S_w \times T_W) + (0.078 \times {T_{ON}}^2) + (0.024 \times {F_R}^2) - (0.018 \times {S_w}^2) + (6.38 \times 10^{-3} \times {T_W}^2) \quad (6)$$

### 3.3.3 Kerf width

ANOVA of KW results for NT and CT wires has been presented in Table 6. From the analysis, it has been observed that the probability values of models are lower than 0.05 which guarantees the significance of developed models. Input variables including $T_{ON}$, $F_R$, $S_W$, and $T_W$ have a significant contribution in KW produced by NT and CT wires. Reasonable values of adequacy measures show the proficiency of developed models. Developed empirical models of KW for both NT and CT wire are given in Eqs. 7 and 8 respectively.

$$\text{Kerf width (NT wire)} = 0.572 - 0.044 \times T_{ON} - 0.017 \times F_R + 2.80 \times 10^{-3} \times S_w - 8.88 \times 10^{-3} \times T_W + (1.33 \times 10^{-3} \times T_{ON} \times F_R) - (8.33 \times 10^{-5} \times T_{ON} \times S_w) + (1.25 \times 10^{-3} \times T_{ON} \times T_W) - (2.77 \times 10^{-5} \times F_R \times S_w) + (1.66 \times 10^{-4} \times F_R \times T_W) - (1.0 \times 10^{-3} \times S_w \times T_W) + (4.84 \times 10^{-3} \times {T_{ON}}^2) + (2.77 \times 10^{-4} \times {F_R}^2) + (5.55 \times 10^{-5} \times {S_w}^2) - (9.58 \times 10^{-4} \times {T_W}^2) \quad (7)$$

$$\text{Kerf width (CT wire)} = 0.894 - 0.066 \times T_{ON} - 0.038 \times F_R - 0.012 \times S_w - 3.96 \times 10^{-3} \times T_W + (2.40 \times 10^{-3} \times T_{ON} \times F_R) - (8.33 \times 10^{-6} \times T_{ON} \times S_w) + (2.45 \times 10^{-3} \times T_{ON} \times T_W) - (2.77 \times 10^{-5} \times F_R \times S_w) + (1.41 \times 10^{-3} \times F_R \times T_W) - (1.37 \times 10^{-3} \times S_w \times T_W) + (4.91 \times 10^{-3} \times {T_{ON}}^2) + (5.42 \times 10^{-4} \times {F_R}^2) + (1.12 \times 10^{-3} \times {S_w}^2) - (1.32 \times 10^{-3} \times {T_W}^2) \quad (8)$$

Table 6. Analysis of variance showing p-values of CS, SR and KW for NT and CT wires

| Source | Cutting speed | | Surface roughness | | Kerf width | | |
|---|---|---|---|---|---|---|---|
| | NT wire | CT wire | NT wire | CT wire | NT wire | CT wire | |
| Model | < 0.0001 | < 0.0001 | < 0.0001 | < 0.0001 | < 0.0001 | < 0.0001 | Significant |
| $T_{ON}$ | < 0.0001 | < 0.0001 | < 0.0001 | < 0.0001 | < 0.0001 | < 0.0001 | |
| $F_R$ | < 0.0001 | < 0.0001 | < 0.0001 | < 0.0001 | < 0.0001 | < 0.0001 | |
| $S_W$ | < 0.0001 | < 0.0001 | 0.0068 | < 0.0001 | < 0.0001 | 0.0004 | |
| $T_W$ | < 0.0001 | < 0.0001 | 0.0007 | < 0.0001 | < 0.0001 | < 0.0001 | |
| $T_{ON} \times F_R$ | 0.0208 | 0.0304 | 0.0212 | 0.0338 | 0.0274 | 0.0144 | |
| $T_{ON} \times S_W$ | 0.0126 | 0.0432 | 0.7513 | 0.6087 | 0.8807 | 0.9925 | |
| $T_{ON} \times T_W$ | 0.1189 | 0.0536 | 0.0197 | < 0.0001 | 0.0369 | 0.0126 | |
| $F_R \times S_W$ | 0.7850 | 0.8315 | 0.3901 | 0.2871 | 0.9401 | 0.9623 | |
| $F_R \times T_W$ | 0.6054 | 0.6867 | 0.5213 | 0.3430 | 0.6534 | 0.0276 | |
| $S_W \times T_W$ | 0.8914 | 0.0339 | 0.0440 | 0.0290 | 0.0149 | 0.0309 | |
| $T_{ON}^2$ | < 0.0001 | 0.0001 | < 0.0001 | < 0.0001 | < 0.0001 | 0.0002 | |
| $F_R^2$ | 0.0001 | < 0.0001 | 0.0359 | < 0.0001 | 0.3333 | 0.2383 | |
| $S_W^2$ | 0.0234 | 0.1876 | 0.0022 | < 0.0001 | 0.8442 | 0.0225 | |
| $T_W^2$ | < 0.0001 | 0.0006 | 0.3863 | 0.0246 | 0.0036 | 0.0088 | |
| Lack of fit | 0.2095 | 0.0833 | 0.1066 | 0.2847 | 0.4030 | 0.1006 | Insignificant |
| Model summary | | | | | | | |
| $R^2$ | 0.993 | 0.989 | 0.966 | 0.988 | 0.967 | 0.947 | |
| $R^2_{Adjusted}$ | 0.986 | 0.979 | 0.933 | 0.976 | 0.935 | 0.898 | |
| $R^2_{Predicted}$ | 0.965 | 0.943 | 0.822 | 0.942 | 0.847 | 0.725 | |
| Adq. precision | 48.322 | 39.432 | 21.575 | 39.346 | 21.848 | 16.438 | |

## 3.4 Multi-objective optimization

WEDM is a susceptible and delicate machining technique that requires intensive surveillance because of its sensitivity toward numerous electrical and non-electrical control parameters. Slight variation in a parameter may result in a convoluted impact on response measure. Therefore, it is inevitable to perform machining without an optimum set of input variables. Mostly, the optimization of a single response is not possible without deteriorating the other responses. However, application of the multi-objective optimization technique has been observed very helpful in the optimization of responses having conflicting nature [62]. In order to increase the CS of workpiece material, both SR and KW also need to be considered together.

### 3.4.1 Grey relational analysis

For multi-response optimization, GRA has been observed as the most effective technique. The technique can analyze multiple parameters at the same time and minimize the deficiencies of primary statistical techniques during analysis. In this technique, response measure values are normalized in the decimals between 0 and 1. For this purpose, three distinct normalizing relations (i) smaller the better, (ii) nominal the best, and (iii) larger the better (Eqs. 9-11) are used according to the nature of response measure [63].

Larger the better $$a_{ij} = \frac{\beta_{ij} - (\beta_{ij})_{min}}{(\beta_{ij})_{max} - (\beta_{ij})_{min}} \quad (9)$$

Nominal the best $$\alpha_{ij} = 1 - \frac{|\beta_{ij} - \beta|}{(\beta_{ij})_{max} - \beta} \quad (10)$$

Smaller the better $$\alpha_{ij} = \frac{(\beta_{ij})_{max} - \beta_{ij}}{(\beta_{ij})_{max} - (\beta_{ij})_{min}} \quad (11)$$

where $\alpha_{ij}$is the *i*th normalized value of *j*th experiment, $\beta_{ij}$ is the measured *i*th response value of *j*th experiment and $\beta$ is the desired/targeted response value. In the case of CS, larger the better function is desirable, and smaller the better objective is preferred for both SR and KW.

To determine the relationship between optimum values and normalized values, grey relational co-efficient has been practiced. Grey relational co-efficient has been calculated using relation (12) given below:

$$\gamma_{ij} = \frac{(\Delta)_{min} + \xi(\Delta)_{max}}{\Delta_{ij} + \xi(\Delta)_{max}} \quad (12)$$

where $\gamma_{ij}$ is the grey relational coefficient of the *i*th normalized value of the *j*th experiment. $\xi$ is the distinguishing co-efficient and its value is generally taken between 0 and 1. In this study, distinguishing co-efficient $\xi$ is taken at 0.5. $\Delta$ is the deviation from the desired/targeted value which is expressed as in Eqs. (13-15) [64]:

$$\Delta_{max} = max_i max_j (y_i^o - y_{ij}) \quad (13)$$

$$\Delta_{min} = min_i min_j (y_i^o - y_{ij}) \quad (14)$$

$$\Delta_{ij} = (y_i^o - y_{ij}) \quad (15)$$

The next step of GRA is the computation of GRG which is the weighting sum of all grey relational coefficients. GRG represents the relationship between input variables and all response measures simultaneously. It is presented in Eq. (16) below:

$$\delta_j = \frac{1}{n} \sum_{i=1}^{n} \gamma_{ij} \quad (16)$$

where $\delta_j$is the GRG of the *j*th experiment and n is the number of response measures (in current study n=3). High GRG value represents the optimal set of input variables for all response measures simultaneously and it is ranked as 1st. For the current study, Table 7 presents the grey relational coefficients, GRG, and their ranking for NT and CT wire electrodes.

Table 7. Multi-objective optimization using GRA for NT and CT wires

| Exp. No. | Grey relational co-efficient (NT wire) | | | Grey relational grade | Rank | Grey relational co-efficient (CT wire) | | | Grey relational grade | Rank |
|---|---|---|---|---|---|---|---|---|---|---|
| | Cutting speed | Surface roughness | Kerf width | | | Cutting speed | Surface roughness | Kerf width | | |
| 1 | 0.339 | 0.689 | 0.403 | 0.477 | 25 | 0.339 | 0.619 | 0.390 | 0.450 | 26 |
| 2 | 0.571 | 0.467 | 0.335 | 0.458 | 28 | 0.556 | 0.425 | 0.334 | 0.438 | 29 |
| 3 | 0.398 | 0.588 | 0.644 | 0.543 | 14 | 0.400 | 0.518 | 0.824 | 0.581 | 4 |
| 4 | 1.000 | 0.333 | 0.381 | 0.571 | 6 | 1.000 | 0.333 | 0.398 | 0.577 | 5 |
| 5 | 0.357 | 0.672 | 0.412 | 0.480 | 24 | 0.362 | 0.603 | 0.406 | 0.457 | 25 |
| 6 | 0.403 | 0.536 | 0.459 | 0.466 | 27 | 0.403 | 0.562 | 0.448 | 0.471 | 24 |
| 7 | 0.389 | 0.722 | 0.528 | 0.547 | 12 | 0.377 | 1.000 | 0.504 | 0.627 | 2 |
| **8** | **0.448** | **0.806** | **1.000** | **0.751** | **1** | **0.493** | **0.683** | **1.000** | **0.725** | **1** |
| 9 | 0.337 | 0.778 | 0.421 | 0.512 | 21 | 0.333 | 0.672 | 0.438 | 0.481 | 22 |
| 10 | 0.574 | 0.381 | 0.350 | 0.435 | 30 | 0.533 | 0.353 | 0.399 | 0.429 | 30 |
| 11 | 0.353 | 0.758 | 0.700 | 0.604 | 2 | 0.349 | 0.645 | 0.811 | 0.602 | 3 |
| 12 | 0.709 | 0.491 | 0.409 | 0.536 | 15 | 0.698 | 0.483 | 0.426 | 0.536 | 9 |
| 13 | 0.384 | 1.000 | 0.392 | 0.592 | 3 | 0.397 | 0.804 | 0.381 | 0.528 | 13 |
| 14 | 0.495 | 0.695 | 0.487 | 0.559 | 10 | 0.518 | 0.588 | 0.475 | 0.527 | 14 |
| 15 | 0.435 | 0.842 | 0.448 | 0.575 | 5 | 0.450 | 0.687 | 0.434 | 0.524 | 17 |
| 16 | 0.574 | 0.544 | 0.583 | 0.567 | 7 | 0.600 | 0.483 | 0.564 | 0.549 | 6 |
| 17 | 0.333 | 0.918 | 0.427 | 0.560 | 9 | 0.336 | 0.853 | 0.415 | 0.534 | 10 |
| 18 | 0.543 | 0.487 | 0.333 | 0.455 | 29 | 0.535 | 0.475 | 0.333 | 0.448 | 27 |
| 19 | 0.358 | 0.777 | 0.500 | 0.545 | 13 | 0.360 | 0.734 | 0.478 | 0.524 | 16 |
| 20 | 0.775 | 0.430 | 0.381 | 0.529 | 18 | 0.743 | 0.422 | 0.372 | 0.513 | 19 |
| 21 | 0.363 | 0.711 | 0.384 | 0.486 | 23 | 0.362 | 0.600 | 0.357 | 0.440 | 28 |
| 22 | 0.459 | 0.470 | 0.491 | 0.473 | 26 | 0.458 | 0.424 | 0.536 | 0.473 | 23 |
| 23 | 0.393 | 0.796 | 0.509 | 0.566 | 8 | 0.391 | 0.663 | 0.578 | 0.544 | 8 |
| 24 | 0.524 | 0.549 | 0.667 | 0.580 | 4 | 0.521 | 0.485 | 0.640 | 0.549 | 7 |
| 25 | 0.437 | 0.674 | 0.491 | 0.534 | 17 | 0.418 | 0.644 | 0.509 | 0.523 | 18 |
| 26 | 0.455 | 0.711 | 0.479 | 0.548 | 11 | 0.430 | 0.676 | 0.496 | 0.534 | 11 |
| 27 | 0.430 | 0.641 | 0.467 | 0.513 | 20 | 0.408 | 0.614 | 0.484 | 0.502 | 20 |
| 28 | 0.435 | 0.674 | 0.496 | 0.535 | 16 | 0.422 | 0.644 | 0.513 | 0.526 | 15 |
| 29 | 0.441 | 0.619 | 0.514 | 0.525 | 19 | 0.426 | 0.630 | 0.531 | 0.529 | 12 |
| 30 | 0.432 | 0.637 | 0.444 | 0.504 | 22 | 0.418 | 0.610 | 0.462 | 0.497 | 21 |

For both NT and CT wire electrodes, the highest GRG values 0.751 and 0.725 have been observed at Exp. No. 08 respectively. Based on the highest GRG values, Exp. No. 08 has been ranked as 1$^{st}$ among all values. This means that best values of CS, SR, and KW can be obtained simultaneously at $T_{ON}$=3 µs, $F_R$=13 m/min, $S_W$=11 m/min, and $T_W$=10 g by trading off responses to a limited extent.

## 3.5 Comparative performance analysis of wire electrodes

Although the response surface graphs have clearly revealed the remarkable performance of the CT wire for CS and SR. To further envision the efficiency of the CT wire electrode, optimum values of CS, SR, and KW have been compared. The percentage increase and decrease of response values of CT wire with respect to NT wire have been displayed in Fig. 13. As maximum CS values are desired, therefore, the comparison has been made at Exp. No. 04 (provided in Table 5). CT wire yields 26.96 % high CS than NT wire. For Ra, the minimum values of both wires are compared at Exp. No. 13. CT wire produces relatively 15.10 % less SR, so the percentage improvement is denoted by a negative sign in Fig. 13. CT wire on the other hand has generated 6.92% higher KW

when its minimum values are analyzed at Exp. No. 08. Based on the above discussion, it can be accomplished that the CT wire electrode is the best candidate for the machining of squeeze casted hybrid AMC.

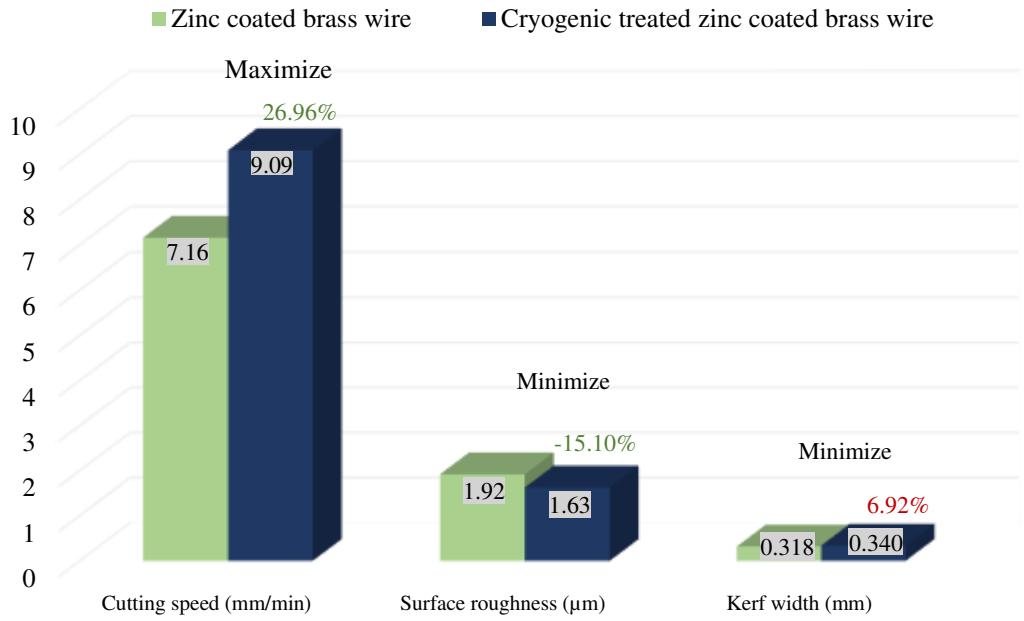


Figure 13. Performance comparison of NT and CT wire electrodes

## 4 Conclusion

This research aims to investigate the selection of potential wire electrode (wire type) and its effects on the machining performance of the squeeze casted Al2024/$Al_2O_3$/W hybrid composite in the WEDM process. To examine the influence of wire type, the machining performance of the cryogenic treated zinc-coated brass wire electrode was compared with simple zinc-coated brass wire. Besides this, the effects of input variables including pulse duration, wire tension, wire feed rate, and wire runoff speed were assessed in terms of cutting speed, surface roughness, and kerf width. Experimental results were analyzed using ANOVA and mathematical models were developed for the response measures (CS, SR, and KW) of both electrode wires. Further, the obtained results of SR and KW were supported by the microstructural analysis. Surface characteristics of both wire electrodes were also evaluated using SEM analysis. GRA was used for the multi-objective optimization of response measures. Based on experimental consequences and findings from their respective discussion, some salient conclusions are figured out:

- The hybrid composite fabricated with the squeeze casting process presents significant mechanical properties (particularly hardness and UTS) and uniform dispersion of particles throughout the metal matrix.
- Cryogenic treatment declined the electrical conductivity of molybdenum wire and improved UTS to a limited extent. On the other hand, the electrical conductivity of zinc-coated brass wire was significantly escalated by 24.8% with cryogenic treatment which depicted the CT brass wire as the potential candidate for machining of squeeze casted Al2024/$Al_2O_3$/W.
- ANOVA showed that $T_{ON}$ as the most significant input variable for the CS, SR, and KW while $F_R$, $T_W$, and $S_W$ were the subsequent substantial input variables for both wires.
- Surface morphology analysis of machined surfaces of AMC characterized that high energy parameters with NT wire generate a surface with a high concentration of micro-voids, globules, deep and larger craters which were reduced by practicing low energy parameters with CT wire.
- SEM analysis revealed that there exists a high concentration of micro-voids and deep craters on the surface of NT wire while shallow craters and a quite smooth surface have been observed in CT wire after machining.
- Multi-objective optimization based on GRA presented $T_{ON}$=3 µs, $F_R$=13 m/min, $S_W$=11 m/min, and $T_W$=10 g as an optimal set of input variables to achieve 75.1% and 72.5% overall results with NT and CT wire respectively by trading off up to a limited extent.
- Comparative analysis of the optimum values of performance measures of wire electrode divulged that CT wire electrode offers 26.96% and 15.10% superior results for CS and SR respectively while 6.92% deprived results for KW than NT wire.

This research proposed suitable wire electrode for the squeeze casted hybrid AMC in the WEDM process, which can be helpful for the practitioners in the machining of such type of material on the industrial scale. Future research can be conducted to analyze the effects of suggested wire type on recast layer thickness, microhardness, and infusion of wire material on the workpiece surface. That study will provide an in-depth analysis of the surface morphology of the workpiece machined with the recommended wire electrode.

**Authors' contributions**

Conceptualization, Methodology, writing original draft: **Muhammad Huzaifa Raza**, Data curation, investigation and visualization: **Muhammad Asad Ali**, Resources and Investigation: **Waseem Tahir,** Supervision and review & editing: **Ray Y. Zhong,** Review & editing: **Nadeem Ahmad Mufti**, Review & editing: **Naveed Ahmad**

**Ethical Approval:** Not applicable

**Consent to Participate:** Not applicable

**Consent to Publish:** Not applicable

**Funding:** This research work was supported in part by the Seed Fund for Basic Research in HKU (Grant No. 201906159001, and in part by ITF project (PRP/068/20LI).

**Competing Interests:** Authors declares no conflict of interest.

**Availability of data and materials:** The paper has no associated data.

## References


1. Pramanik, A., Effects of reinforcement on wear resistance of aluminum matrix composites. Transactions of Nonferrous Metals Society of China, 2016. **26**(2): p. 348-358.
2. Dinaharan, I., et al., Microstructure and wear characterization of aluminum matrix composites reinforced with industrial waste fly ash particulates synthesized by friction stir processing. Materials Characterization, 2016. **118**: p. 149-158.
3. Xie, X., et al., Achieving simultaneously improved tensile strength and ductility of a nano-TiB2/AlSi10Mg composite produced by cold spray additive manufacturing. Composites Part B: Engineering, 2020. **202**: p. 108404.
4. Zhang, C., et al., Enhanced tensile properties of Al matrix composites reinforced with β-Si3N4 whiskers. Composites Part A: Applied Science and Manufacturing, 2017. **102**: p. 145-153.
5. Akinwamide, S.O., O.J. Akinribide, and P.A. Olubambi, Microstructural evolution, mechanical and nanoindentation studies of stir cast binary and ternary aluminium based composites. Journal of Alloys and Compounds, 2021. **850**: p. 156586.
6. Idrisi, A.H. and A.-H.I. Mourad, Conventional stir casting versus ultrasonic assisted stir casting process: Mechanical and physical characteristics of AMCs. Journal of Alloys and Compounds, 2019. **805**: p. 502-508.
7. Lee, D., et al., Experimental and thermodynamic study on interfacial reaction of B4C–Al6061 composites fabricated by stir casting process. Journal of Alloys and Compounds, 2020: p. 157813.
8. Sarfraz, M.H., et al., Multi-response parametric optimization of squeeze casting process for fabricating Al 6061-SiC composite. The International Journal of Advanced Manufacturing Technology, 2019. **102**(1): p. 759-773.
9. Liao, Z., et al., State-of-the-art of surface integrity in machining of metal matrix composites. International Journal of Machine Tools and Manufacture, 2019. **143**: p. 63-91.
10. Senthil, P., T. Selvaraj, and K. Sivaprasad, Influence of turning parameters on the machinability of homogenized Al–Cu/TiB 2 in situ metal matrix composites. The International Journal of Advanced Manufacturing Technology, 2013. **67**(5-8): p. 1589-1596.
11. Bejjani, R., et al., Chip formation and microstructure evolution in the adiabatic shear band when machining titanium metal matrix composites. International Journal of Machine Tools and Manufacture, 2016. **109**: p. 137-146.
12. Pugazhenthi, A., et al., Turning characteristics of in situ formed TiB2 ceramic particulate reinforced AA7075 aluminum matrix composites using polycrystalline diamond cutting tool. Measurement, 2018. **121**: p. 39-46.
13. Dandekar, C.R. and Y.C. Shin, Modeling of machining of composite materials: A review. International Journal of Machine Tools and Manufacture, 2012. **57**: p. 102-121.
14. Nicholls, C.J., et al., Review of machining metal matrix composites. The International Journal of Advanced Manufacturing Technology, 2017. **90**(9-12): p. 2429-2441.
15. Raju, R., et al., Optimization of process parameters in Electrical Discharge Machining of Haste Alloy C276 using Taguchi's method. Materials Today: Proceedings, 2018. **5**(6, Part 2): p. 14432-14439.
16. Reolon, L.W., et al., WEDM performance and surface integrity of Inconel alloy IN718 with coated and uncoated wires. The International Journal of Advanced Manufacturing Technology, 2019. **100**(5-8): p. 1981-1991.
17. Tahir, W. and M. Jahanzaib, Multi-objective optimization of WEDM using cold treated brass wire for HSLA hardened steel. Journal of the Brazilian Society of Mechanical Sciences and Engineering, 2019. **41**(11): p. 525.
18. Gong, Y., et al., Experimental study on surface integrity of Ti-6Al-4V machined by LS-WEDM. The International Journal of Advanced Manufacturing Technology, 2017. **88**(1): p. 197-207.
19. Paswan, K., A. Pramanik, and S. Chattopadhyaya, Machining performance of Inconel 718 using graphene nanofluid in EDM. Materials and Manufacturing Processes, 2020. **35**(1): p. 33-42.
20. Muniappan, A., et al., Optimization of WEDM Process Parameters for Cutting Speed using Taguchi technique. Materials Today: Proceedings, 2019. **18**: p. 332-341.
21. Satishkumar, D. and M. Kanthababu, Optimization of Wedm Parameters for Surface Roughness on Hybrid Mmcs. Advanced Composites Letters, 2014. **23**(3): p. 096369351402300303.
22. Ugrasen, G., et al., Estimation of Machining Performances using MRA and GMDH in Wire EDM of Al2024 based Hybrid MMC. Materials Today: Proceedings, 2018. **5**(1, Part 3): p. 3084-3092.
23. Nag, A., et al., Surface Integrity analysis of Wire-EDM on in-situ hybrid composite A359/Al2O3/B4C. Materials Today: Proceedings, 2018. **5**(11, Part 3): p. 24632-24641.
24. Kumar, S.S., et al., Parametric optimization of wire electrical discharge machining on aluminium based composites through grey relational analysis. Journal of Manufacturing Processes, 2015. **20**: p. 33-39.
25. Udaya Prakash, J., et al., Optimization of Wire EDM Process Parameters for Machining Hybrid Composites (356/B4C/Fly Ash) using Taguchi Technique. Materials Today: Proceedings, 2018. **5**(2, Part 2): p. 7275-7283.
26. Lal, S., et al., Wire electrical discharge machining of AA7075/SiC/Al2O3 hybrid composite fabricated by inert gas-assisted electromagnetic stir-casting process. Journal of the Brazilian Society of Mechanical Sciences and Engineering, 2014. **36**(2): p. 335-346.
27. Ishfaq, K., et al., Optimization of WEDM for precise machining of novel developed Al6061-7.5% SiC squeeze-casted composite. The International Journal of Advanced Manufacturing Technology, 2020.

28. Tahir, W., M. Jahanzaib, and A. Raza, Effect of process parameters on cutting speed of wire EDM process in machining HSLA steel with cryogenic treated brass wire. Advances in Production Engineering & Management, 2019. **14**(2): p. 143-152.
29. Goyal, A., Investigation of material removal rate and surface roughness during wire electrical discharge machining (WEDM) of Inconel 625 super alloy by cryogenic treated tool electrode. Journal of King Saud University-Science, 2017. **29**(4): p. 528-535.
30. Özbek, N.A., et al., Investigation of the effects of cryogenic treatment applied at different holding times to cemented carbide inserts on tool wear. International Journal of Machine Tools and Manufacture, 2014. **86**: p. 34-43.
31. Yao, Y. and Y. Zhou, Effects of deep cryogenic treatment on wear resistance and structure of GB 35CrMoV steel. Metals, 2018. **8**(7): p. 502.
32. Senthilkumar, D. and I. Rajendran, Optimization of deep cryogenic treatment to reduce wear loss of 4140 steel. Materials and Manufacturing Processes, 2012. **27**(5): p. 567-572.
33. Li, G.R., et al., The influence of cryogenic-aging circular treatment on the microstructure and properties of aluminum matrix composites. Journal of Alloys and Compounds, 2017. **695**: p. 1930-1945.
34. Seah, K., M. Rahman, and K. Yong, Performance evaluation of cryogenically treated tungsten carbide cutting tool inserts. Proceedings of the Institution of Mechanical Engineers, Part B: Journal of Engineering Manufacture, 2003. **217**(1): p. 29-43.
35. Kapoor, J., J.S. Khamba, and S. Singh, Effect of shallow cryogenic treated brass wire electrode on workpiece surface roughness in wire-EDM. International Journal of Materials Engineering Innovation, 2012. **3**(3-4): p. 190-203.
36. Kapoor, J., S. Singh, and J.S. Khamba, Effect of cryogenic treated brass wire electrode on material removal rate in wire electrical discharge machining. Proceedings of the Institution of Mechanical Engineers, Part C: Journal of Mechanical Engineering Science, 2012. **226**(11): p. 2750-2758.
37. Nayak, B.B. and S.S. Mahapatra, Optimization of WEDM process parameters using deep cryo-treated Inconel 718 as work material. Engineering Science and Technology, an International Journal, 2016. **19**(1): p. 161-170.
38. Goyal, A., Investigation of material removal rate and surface roughness during wire electrical discharge machining (WEDM) of Inconel 625 super alloy by cryogenic treated tool electrode. Journal of King Saud University - Science, 2017. **29**(4): p. 528-535.
39. Raza, M.H., et al., Investigating the effects of different electrodes on Al6061-SiC-7.5 wt% during electric discharge machining. The International Journal of Advanced Manufacturing Technology, 2018. **99**(9): p. 3017-3034.
40. Kapoor, J., S. Singh, and J.S.J.P.o.t.I.o.M.E. Khamba, Part C: Journal of Mechanical Engineering Science, Effect of cryogenic treated brass wire electrode on material removal rate in wire electrical discharge machining. 2012. **226**(11): p. 2750-2758.
41. Bankole, M.T., et al., Optimization of supported bimetallic (Fe-Co/CaCO3) catalyst synthesis parameters for carbon nanotubes growth using factorial experimental design. Journal of Alloys and Compounds, 2018. **749**: p. 85-102.
42. Raza, M.H., et al., Investigation of surface roughness in face milling processes. 2020. **111**(9): p. 2589-2599.
43. Raza, M.H., et al., Investigating the effects of gating design on mechanical properties of aluminum alloy in sand casting process. 2020.
44. Akhtar, M.U., M.H. Raza, and M.J.J.o.I.E.I. Shafiq, Role of batch size in scheduling optimization of flexible manufacturing system using genetic algorithm. 2019. **15**(1): p. 135-146.
45. Rajabloo, T., et al., Taguchi based fuzzy logic optimization of multiple quality characteristics of cobalt disulfide nanostructures. Journal of Alloys and Compounds, 2014. **607**: p. 61-66.
46. Gao, T.J., et al., Strain-rate-sensitive mechanical response, twinning, and texture features of NiCoCrFe high-entropy alloy: Experiments, multi-level crystal plasticity and artificial neural networks modeling. Journal of Alloys and Compounds, 2020. **845**: p. 155911.
47. Montgomery, D.C., Design and analysis of experiments. 2017: John wiley & sons.
48. Ali, M.A., et al., Evaluating the effects of as-casted and aged overcasting of Al-Al joints. The International Journal of Advanced Manufacturing Technology, 2018. **96**(1): p. 1377-1392.
49. Kavimani, V., K.S. Prakash, and T. Thankachan, Multi-objective optimization in WEDM process of graphene–SiC-magnesium composite through hybrid techniques. Measurement, 2019. **145**: p. 335-349.
50. Gopal, P.M., K.S. Prakash, and S. Jayaraj, WEDM of Mg/CRT/BN composites: Effect of materials and machining parameters. Materials and Manufacturing Processes, 2018. **33**(1): p. 77-84.
51. Rajmohan, K. and A.S. Kumar, Experimental investigation and prediction of optimum process parameters of micro-wire-cut EDM of 2205 DSS. The International Journal of Advanced Manufacturing Technology, 2017. **93**(1-4): p. 187-201.
52. Habib, S. and A. Okada, Experimental investigation on wire vibration during fine wire electrical discharge machining process. The International Journal of Advanced Manufacturing Technology, 2016. **84**(9): p. 2265-2276.
53. Chen, Z., et al., Theoretical and experimental study of magnetic-assisted finish cutting ferromagnetic material in WEDM. International Journal of Machine Tools and Manufacture, 2017. **123**: p. 36-47.

54. Manjaiah, M., et al., Effect of electrode material in wire electro discharge machining characteristics of Ti50Ni50−xCux shape memory alloy. Precision Engineering, 2015. **41**: p. 68-77.
55. Kumar, S.S., et al., Investigation of WEDM process parameters of Al–SiC–B4C composites using response surface methodology. International Journal of Lightweight Materials and Manufacture, 2019.
56. Habib, S., Optimization of machining parameters and wire vibration in wire electrical discharge machining process. Mechanics of Advanced Materials and Modern Processes, 2017. **3**(1): p. 3.
57. Habib, S. and A. Okada, Study on the movement of wire electrode during fine wire electrical discharge machining process. Journal of Materials Processing Technology, 2016. **227**: p. 147-152.
58. Tahir, W., et al., Surface morphology evaluation of hardened HSLA steel using cryogenic-treated brass wire in WEDM process. 2019. **104**(9-12): p. 4445-4455.
59. Krishnaiah, K. and P. Shahabudeen, Applied design of experiments and Taguchi methods. 2012: PHI Learning Pvt. Ltd.
60. Raza, M.H., et al., Modeling of the mechanical properties of directionally solidified Al-4.3% Cu alloy using response surface methodology. The International Journal of Advanced Manufacturing Technology, 2019: p. 1-13.
61. Ali, M.A., et al., Mechanical characterization of aged AA2026-AA2026 overcast joints fabricated by squeeze casting. The International Journal of Advanced Manufacturing Technology, 2020: p. 1-21.
62. Yuan, J., et al., Reliable multi-objective optimization of high-speed WEDM process based on Gaussian process regression. International Journal of Machine Tools and Manufacture, 2008. **48**(1): p. 47-60.
63. Ishfaq, K., et al., Evaluating Material's Interaction in Wire Electrical Discharge Machining of Stainless Steel (304) for Simultaneous Optimization of Conflicting Responses. Materials, 2019. **12**(12): p. 1940.
64. Wojciechowski, S., et al., Application of signal to noise ratio and grey relational analysis to minimize forces and vibrations during precise ball end milling. Precision Engineering, 2018. **51**: p. 582-596.

# Figures

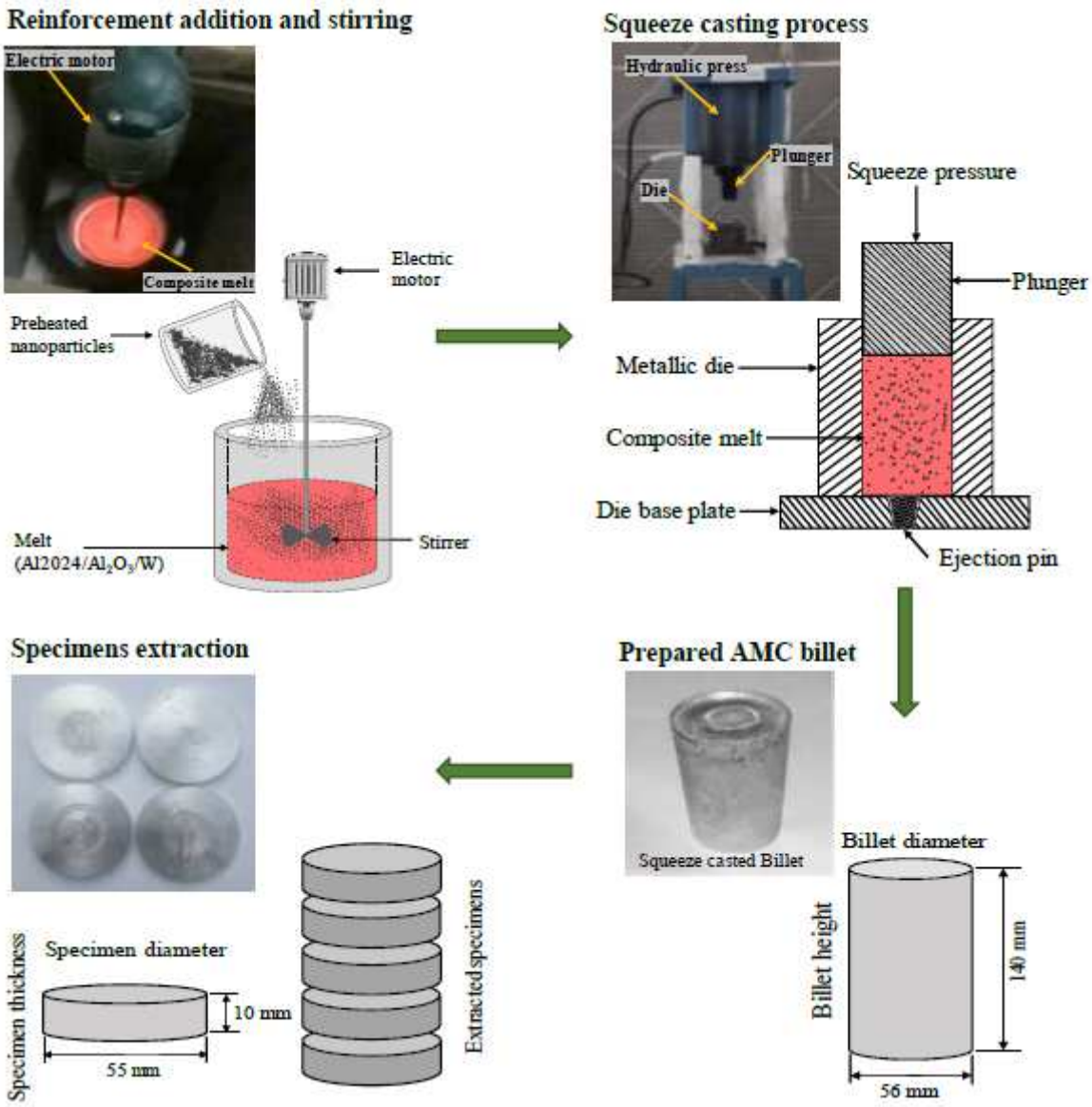


**Figure 1**

Hybrid AMC specimens' preparation through the squeeze casting process and its schematic illustration

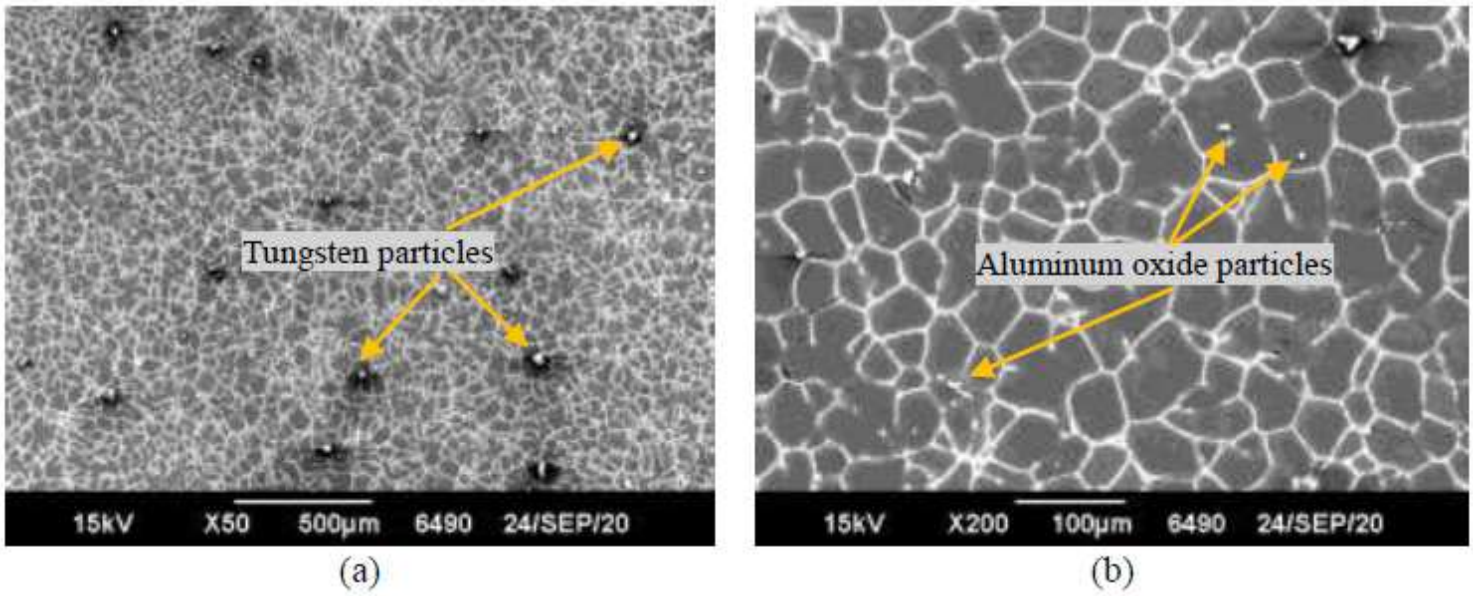


**Figure 2**

Microstructure of squeeze casted composite material showing (a) large sized tungsten and (b) comparatively smaller sized Al2O3 nanoparticles shown at the higher resolution


## Figure 3

Framework for the selection of appropriate wire electrode for the machining of the squeeze casted Al2024/Al2O3/W hybrid composite

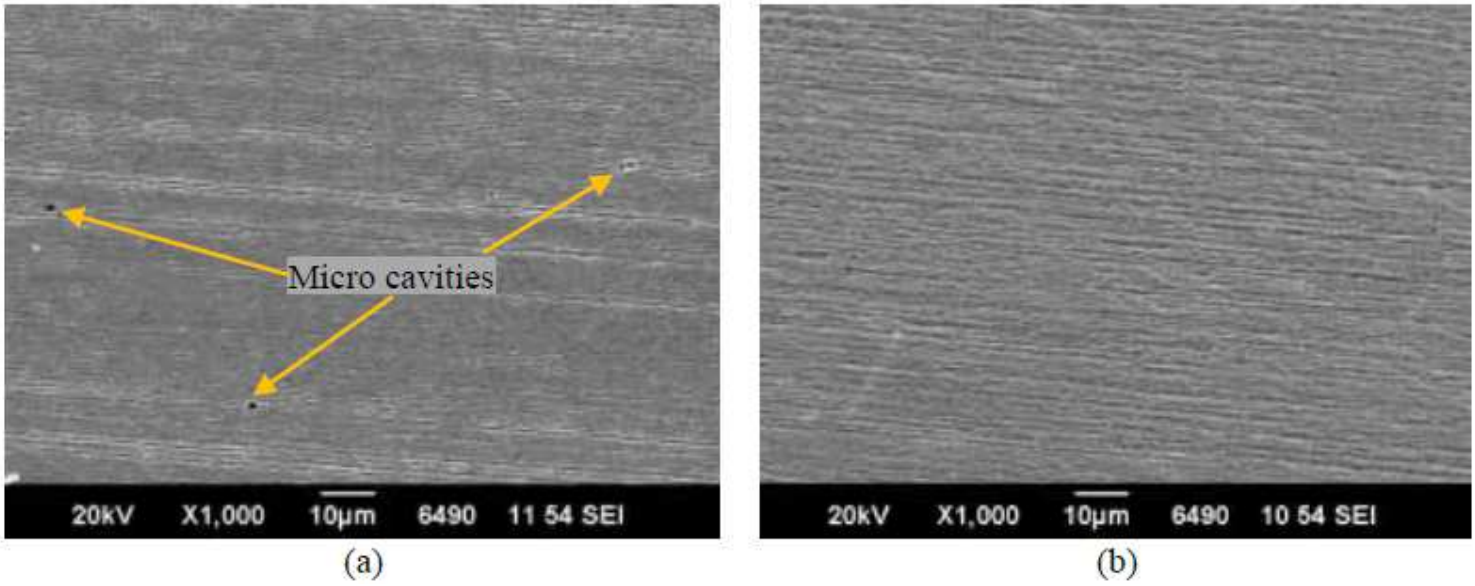


**Figure 4**

Microstructure of (a) non-treated and (b) cryogenically treated brass wire

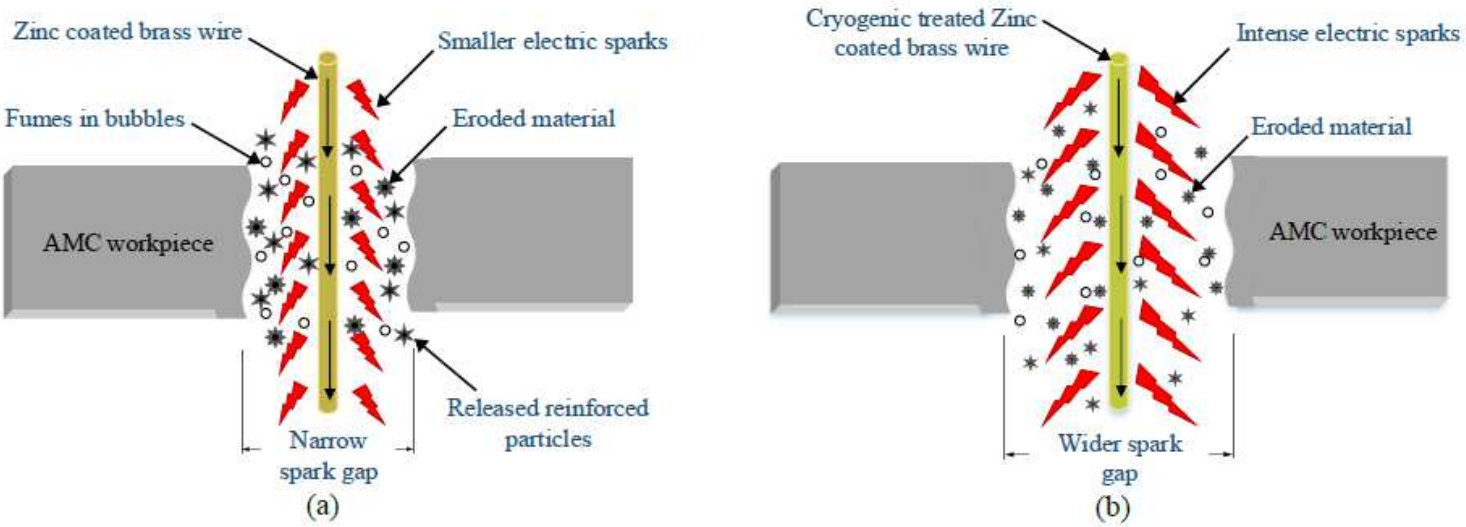


**Figure 5**

Schematic illustration of the machining of AMC with (a) simple zinc coated brass wire (b) cryogenic treated zinc coated brass wire

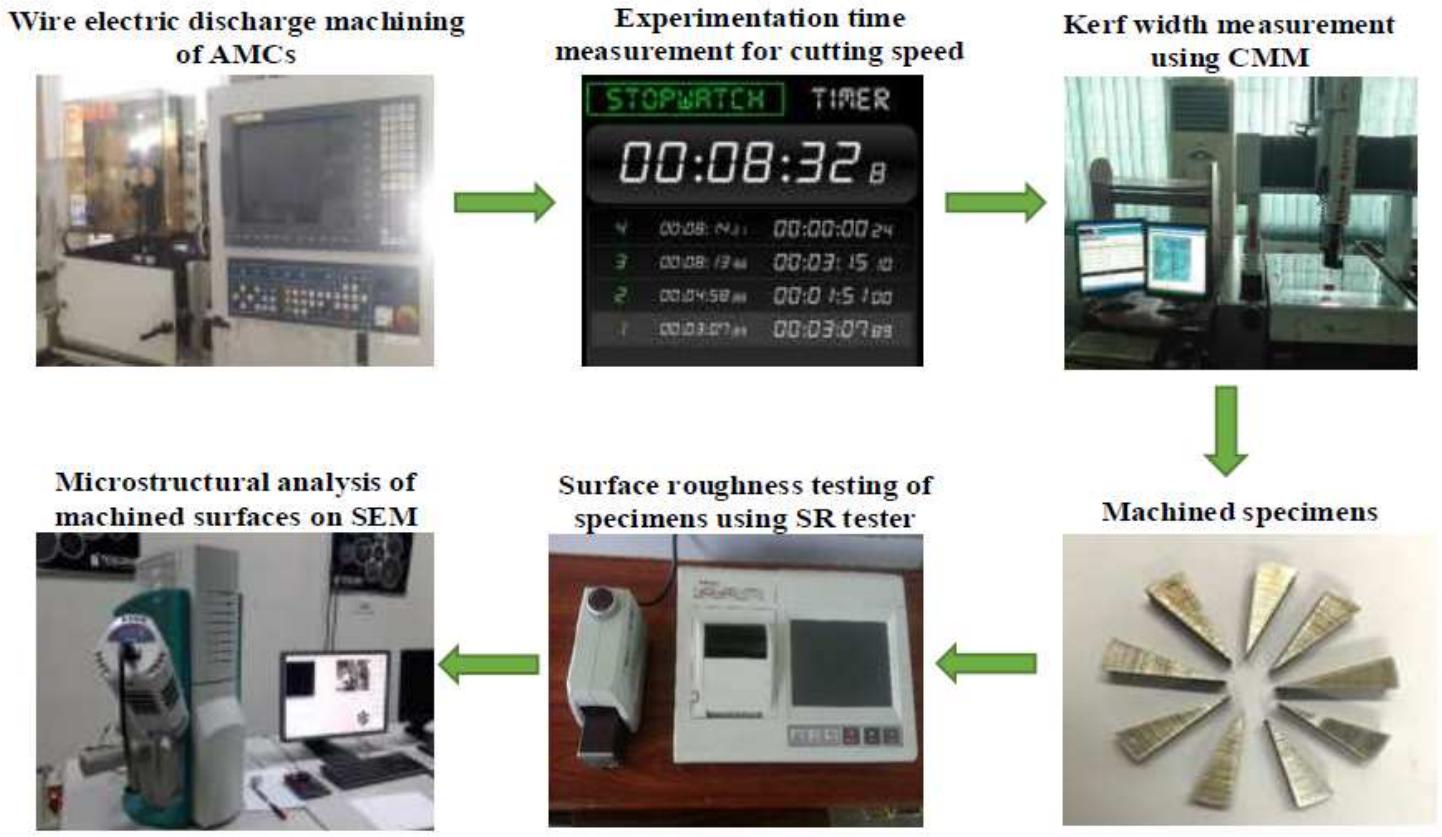


## Figure 6

Experimental procedure and response measurement

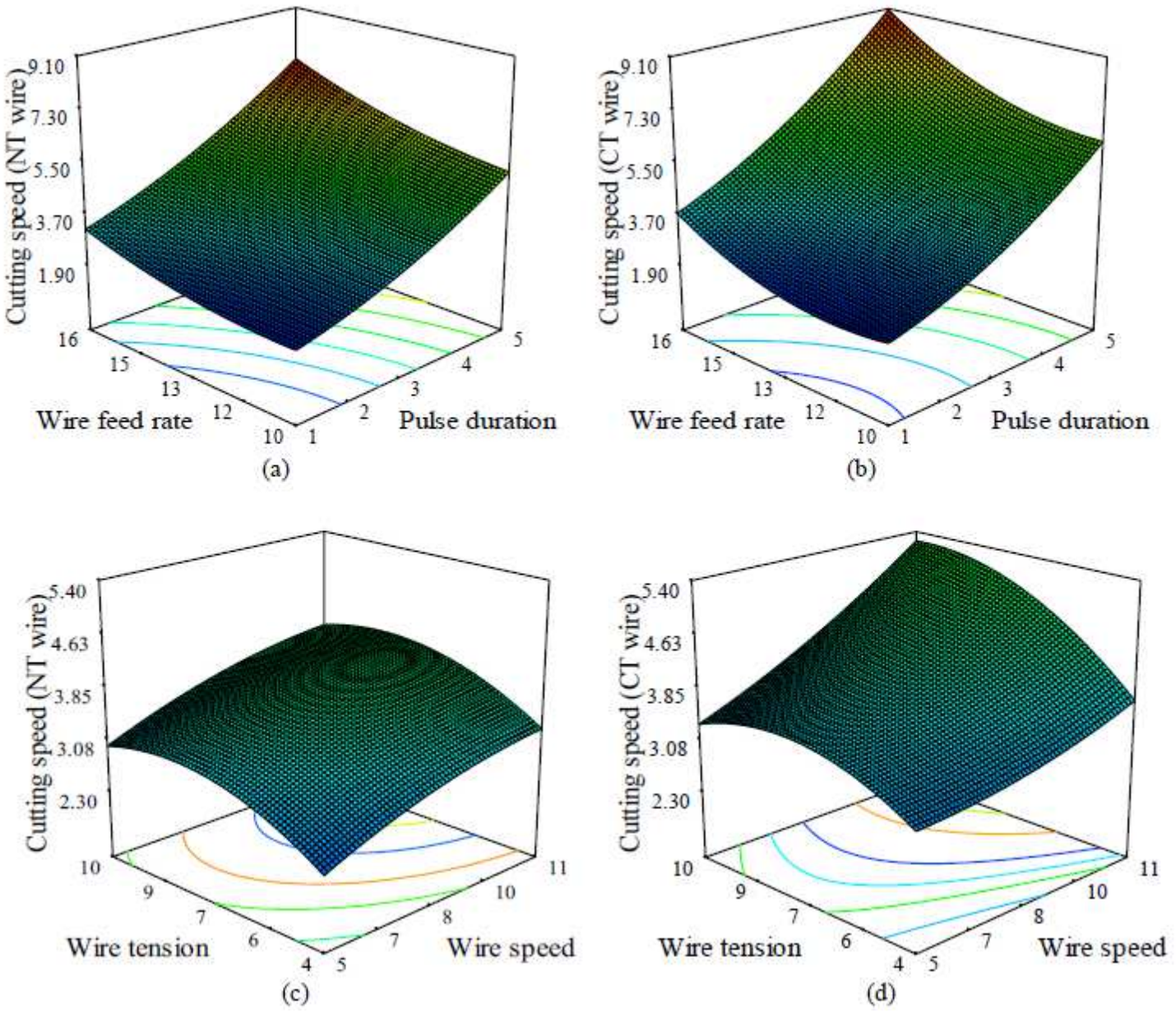


## Figure 7

3D response surface graphs presenting the effects of TON and FR on CS for (a) NT wire (b) CT wire and SW and TW on CS for (c) NT wire and (d) CT wire

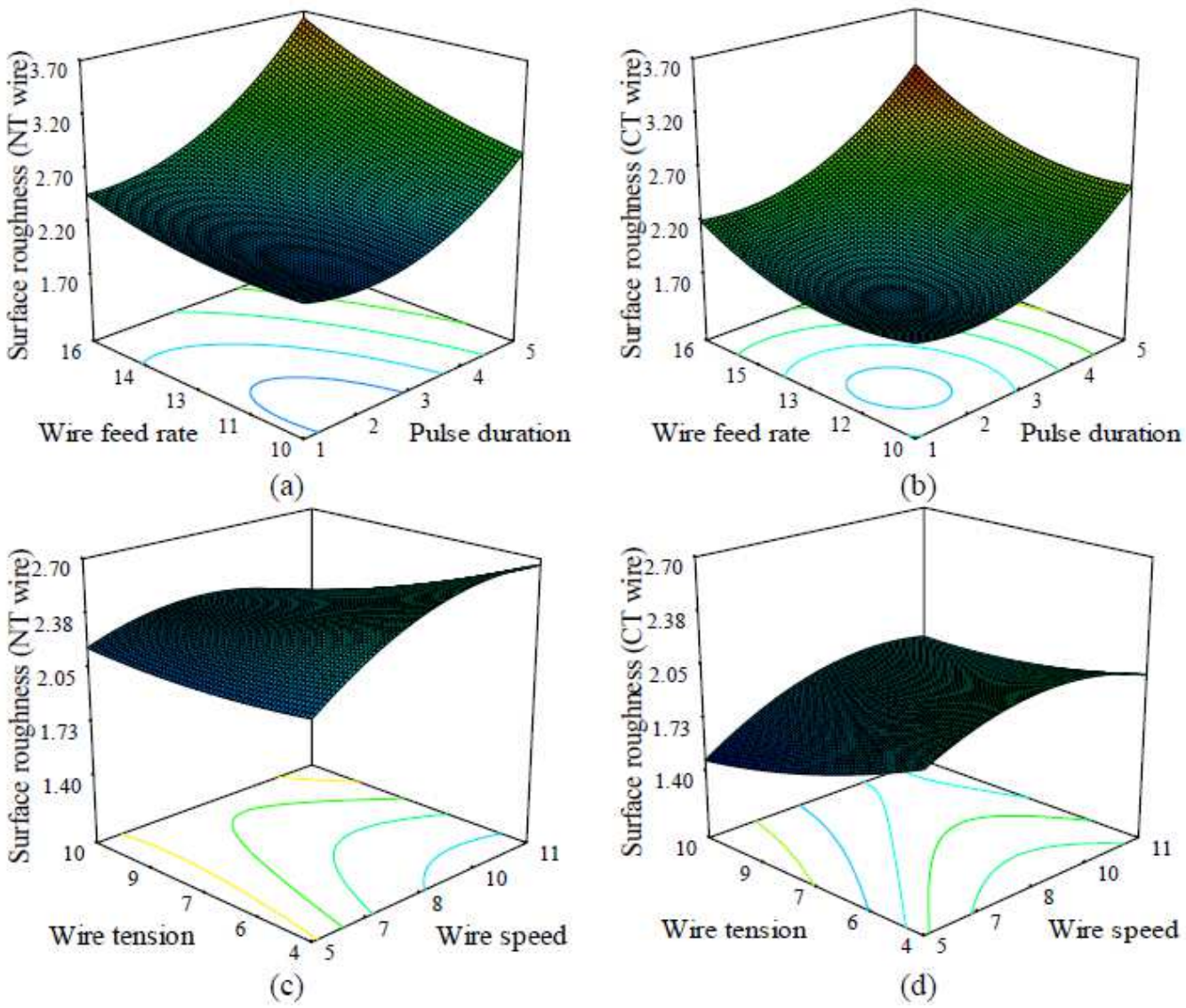


## Figure 8

3D response surface graph for the effects of TON and FR on SR for (a) NT wire (b) CT wire and SW and TW on SR for (c) NT wire and (d) CT wire

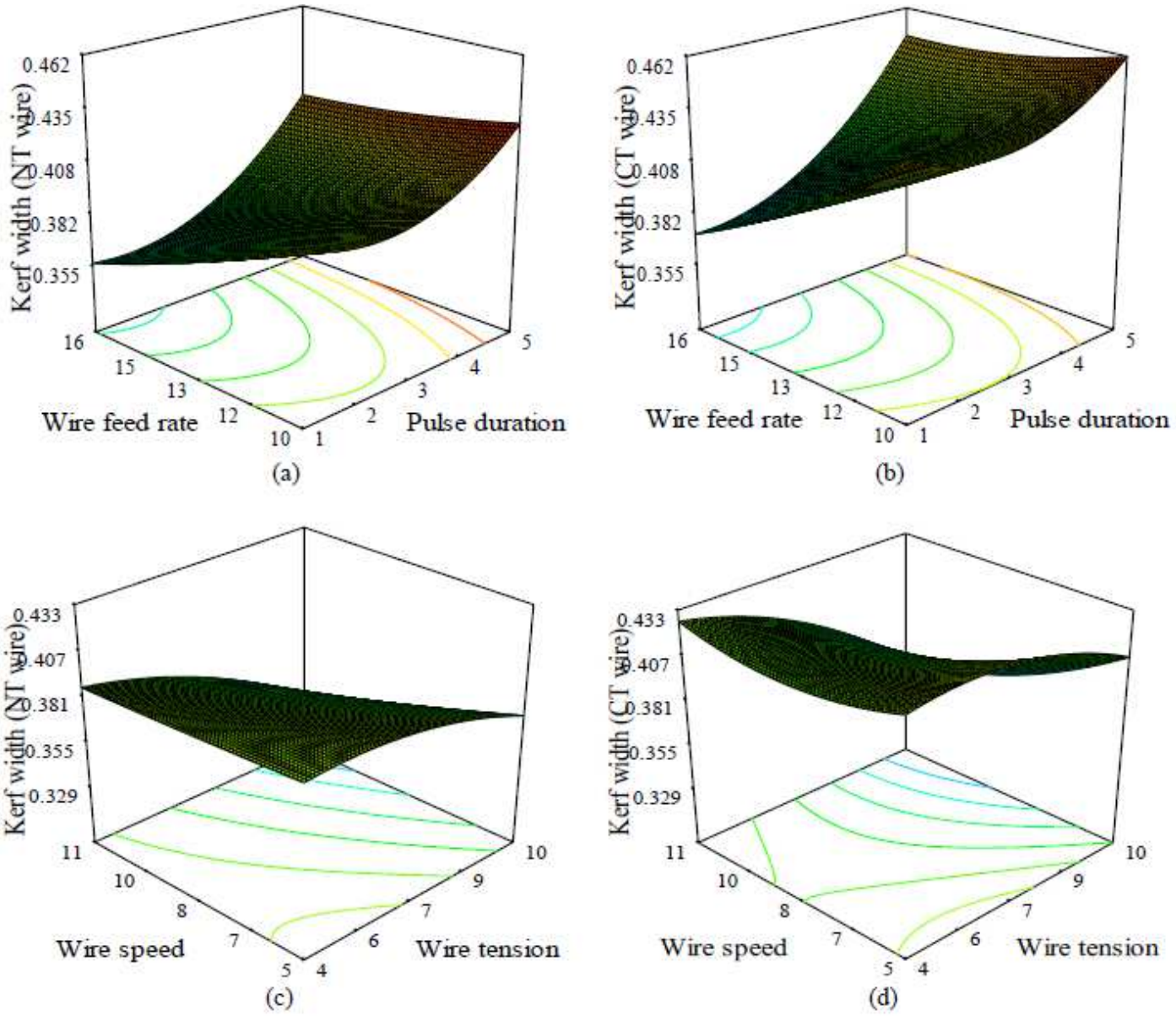


## Figure 9

3D response surface graph showing the influence of TON and FR on KW for (a) NT wire (b) CT wire and SW and TW on KW for (c) NT wire and (d) CT wire

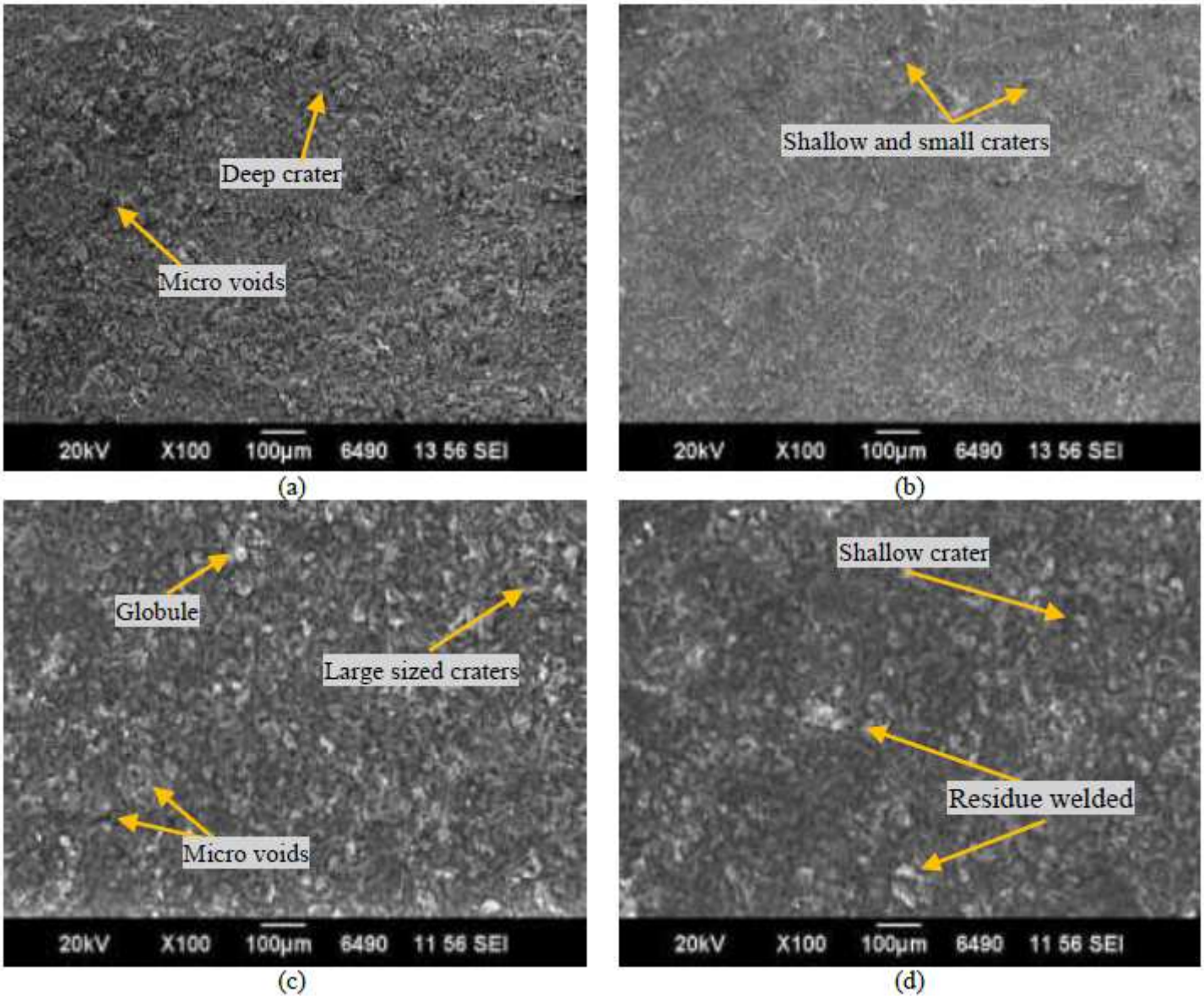


**Figure 10**

Microstructure of the machined surfaces at Exp. No. 13 for (a) NT (b) CT wires and Exp. No. 04 for (c) NT (d) CT wires

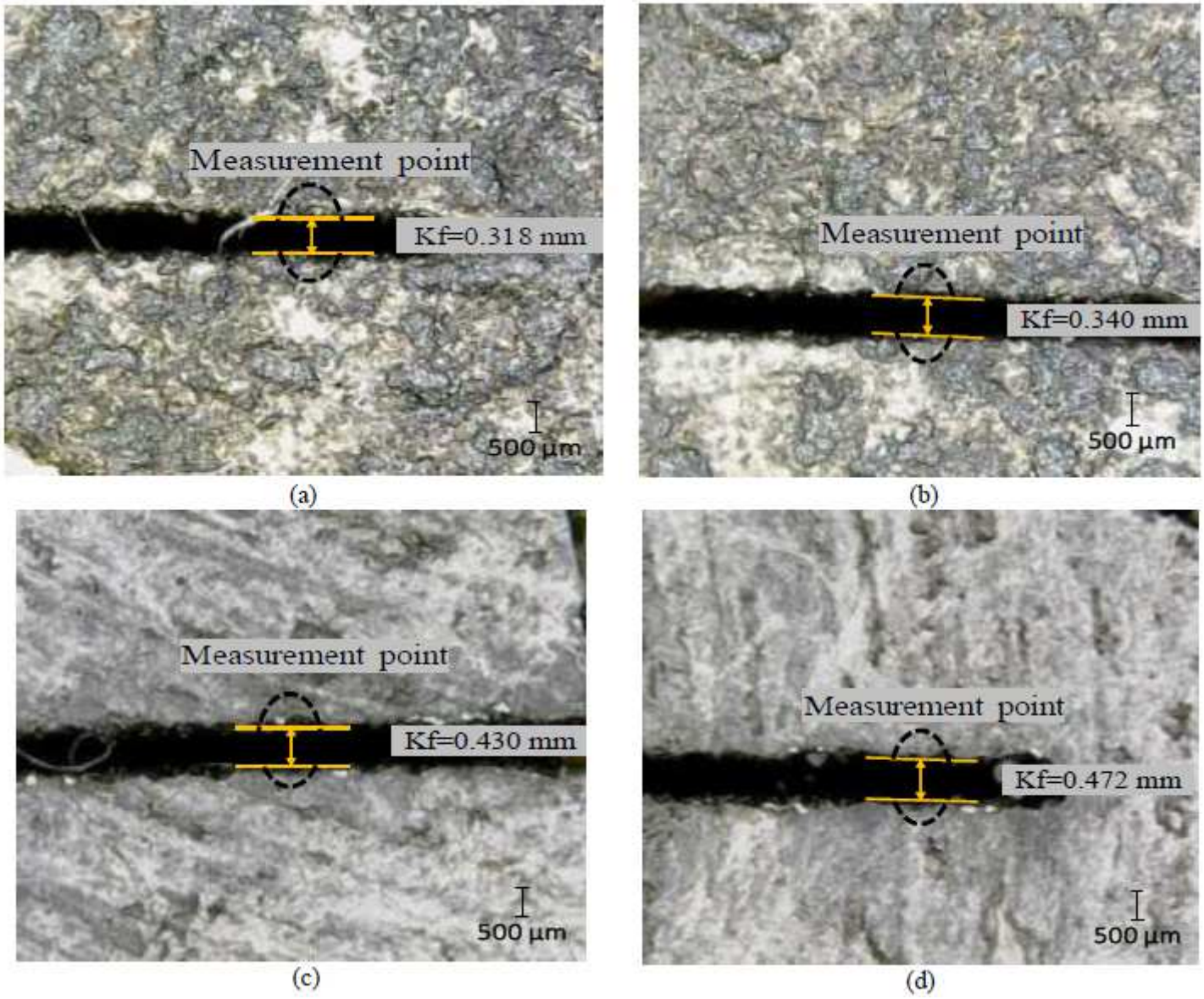


**Figure 11**

Micrograph showing minimum KW values at Exp. No. 08 using (a) NT wire, (b) CT wire, and maximum KW values at Exp. No. 18 with (c) NT wire and (d) CT wire

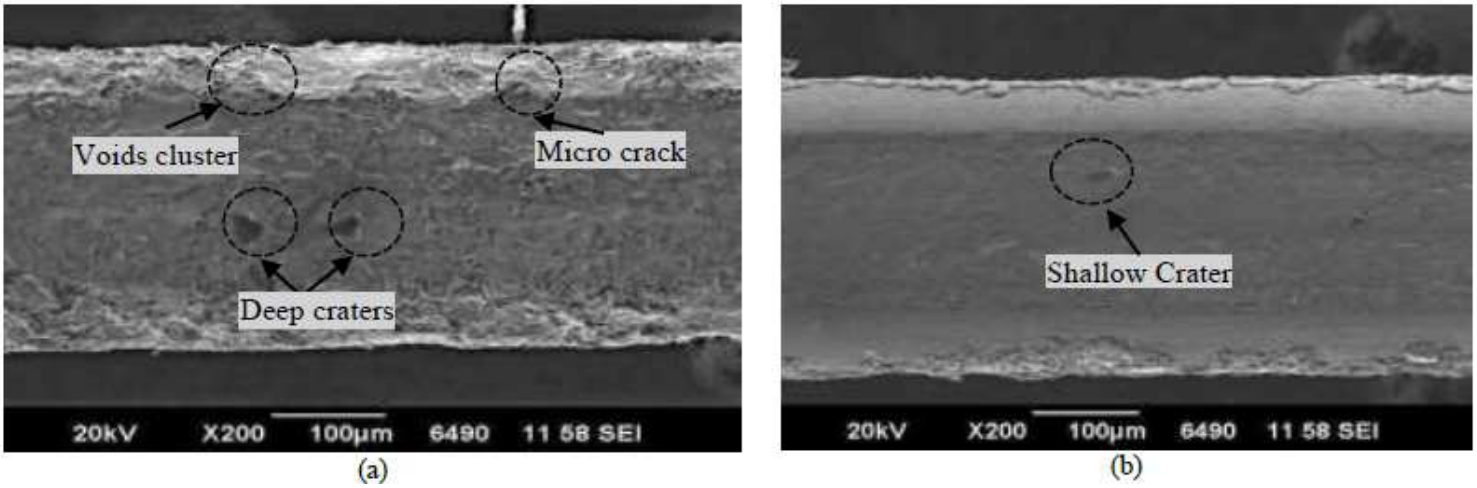

**Figure 12**

Microstructure of (a) NT and (b) CT wire after experimentation

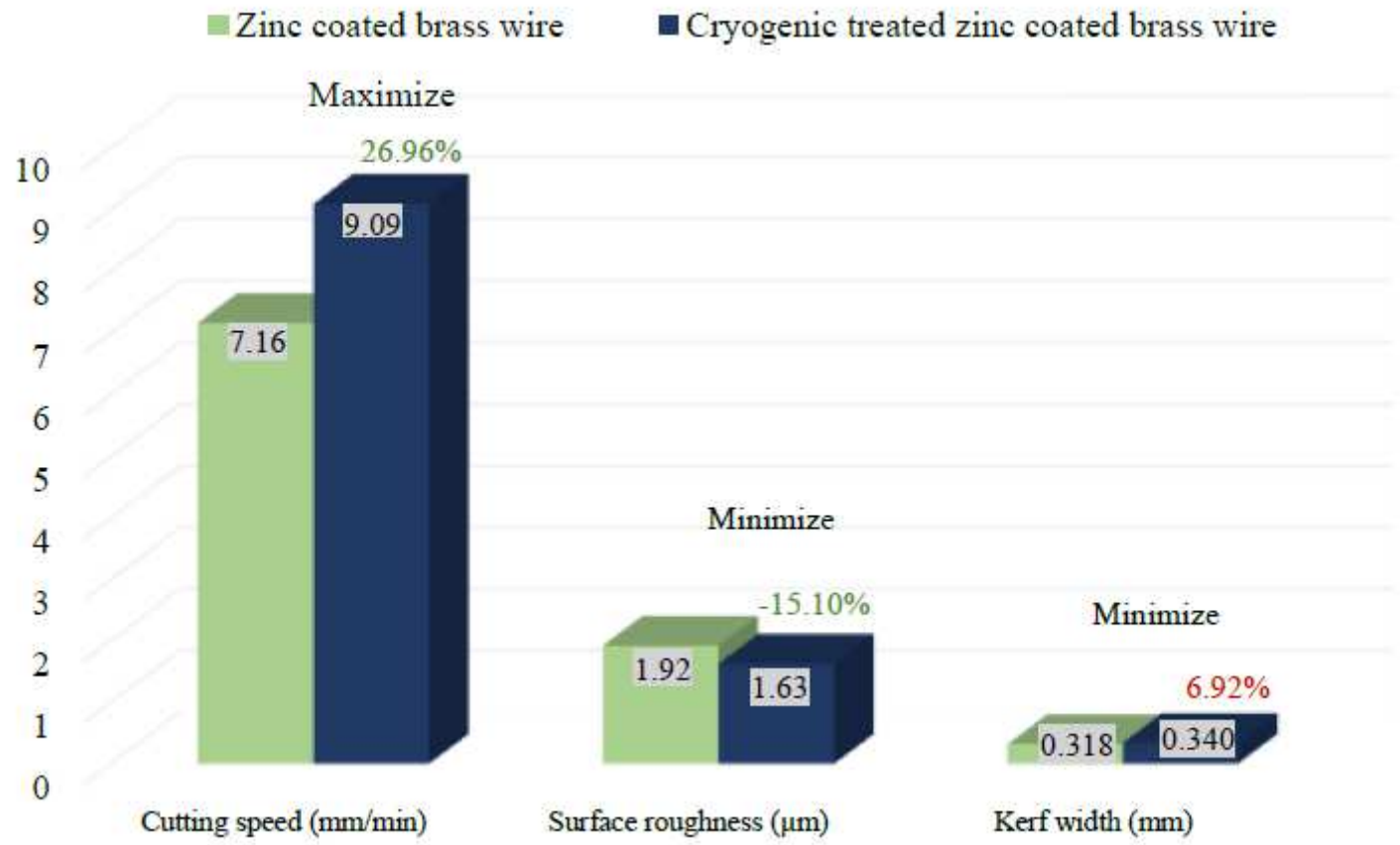


**Figure 13**

Performance comparison of NT and CT wire electrodes